Wall-Resolved Spectral Cascade-Transport Turbulence Model

C.S. Brown[1*]; D.R. Shaver[2]; R.T. Lahey, Jr.[3]; I.A. Bolotnov[1]
[1]*Department of Nuclear Engineering, North Carolina State University*
Campus Box 7909, Raleigh, NC, USA 27695-7909
[2]*NE Division, Argonne National Laboratory*
Argonne, IL, USA 60439
[3]*Department of Mechanical, Aerospace and Nuclear Engineering, Rensselaer Polytechnic Institute*
Troy, NY, USA 12180
[*]csbrown3@ncsu.edu

ABSTRACT

A spectral cascade-transport model has been developed and applied to turbulent channel flows (Re_τ= 550, 950, and 2000 based on friction velocity, u_τ; or Re_δ= 8,500; 14,800 and 31,000, based on the mean velocity and channel half-width). This model is an extension of a spectral model previously developed for homogeneous single and two-phase decay of isotropic turbulence and uniform shear flows; and a spectral turbulence model for wall-bounded flows without resolving the boundary layer. Data from direct numerical simulation (DNS) of turbulent channel flow was used to help develop this model and to assess its performance in the 1D direction across the channel width. The resultant spectral model is capable of predicting the mean velocity, turbulent kinetic energy and energy spectrum distributions for single-phase wall-bounded flows all the way to the wall, where the model source terms have been developed to account for the wall influence. The model has been implemented into the 3D multiphase CFD code NPHASE-CMFD and the latest results are within reasonable error of the 1D predictions.

KEYWORDS
spectral-cascade, spectral turbulence model, channel flow, DNS, CFD

1 INTRODUCTION

There are numerous Reynolds-averaged Navier-Stokes (RANS) type turbulence models in the literature but all of them have well known limitations (WILCOX, 2002). However, the continually increasing computational capabilities to perform direct numerical simulation (DNS) (Bolotnov et al., 2008a,Trofimova et al., 2009,Del Alamo et al., 2004,del Alamo and Jimenez, 2003,Hoyas and Jimenez, 2006,Fang et al., 2016) provides detailed results that can be used to assess existing turbulence modeling approaches as well as to develop a more physically-based spectral turbulence model. High fidelity computational fluid dynamic (CFD) simulations improve nuclear reactor safety and operation calculations. Moreover, multiphase computational fluid dynamics (M-CFD) remains a challenging problem in engineering and the multiphase flow models in reactor relevant applications must account for complex geometries within the reactor core. More physically based M-CFD simulations of the intricate flow scenarios in nuclear reactor subchannels around spacer grids, mixing vanes, fuel bundles, etc. will deliver better predictions of flow characteristics such as three-dimensional void fraction and velocity distributions. Spectral turbulence models provide more flow statistics than traditional two-equation models (i.e. the turbulent kinetic energy (TKE) spectrum) and are a good choice for M-CFD since bubble source terms can be modeled as contributions to specific turbulence scales.

Some earlier spectral considerations to the modeling of turbulence involved the so-called multiple-time-scale models (Bradbury et al., 1980). The TKE spectrum was split into two or more scales, and each scale was modeled using a separate set of equations (such as k-ε) accounting for the interaction of these scales. Schiestel (1987) used Kovasznay hypothesis (Hinze, 1975) to model the spectral transfer in multiple-time-scale models based on partial integration of the spectral evolution equations. This spectral term is also used in the presented work.

Kim & Chen (1989) introduced a variable partitioning of the two scales which allowed a constant distribution of energy between the scales in different parts of the spatial domain. Kim (1990) extended the multiple-time-scale model all the way to the wall to obtain the low-Reynolds-number model by using a new wall damping function. Note that these models still used a dissipation rate equation for both scales and had a different set of model coefficients for each scale.

Spectral transport models split the TKE into interacting spectral bins with a separate transport equation solved for each bin. This type of spectral model can be classified as a shell model (Bohr et al., 1998). The idea to use spectral shells in the modeling of turbulent energy cascade was proposed by Desnyanski & Novikov (1974). They reproduced the Kolmogorov spectrum in terms of appropriate ordinary differential equations (ODE) for the averaged velocity field in Fourier space. The so-called GOY model (after Gledzer (1973), Ohkitani and Yamada (1989)) used a complex variable per shell and

featured interactions between nearest and next-nearest neighboring shells, maintaining energy and volume concentration in phase space. Following Desnyanski and Novikov, Lewalle and Tavlarides (1994) developed the cascade-transport (CT) model and performed calibration and testing with homogeneous uniform shear flow experimental data. In their CT model, energy is exchanged between the nearest modes only, the dissipation term is explicit (without the need for an additional dissipation rate transport equation such as in k-ε type models), and the diffusion and production terms match those in the model TKE equation. Lewalle and Tavlarides (1994) used a cumulative spectral eddy viscosity model given by Heisenberg (see Hinze (1975)) to formulate the CT model eddy viscosity with a correction factor used outside of the inertial subrange. The CT model achieved good agreement with the experimental results although the authors note that the solution had considerable sensitivity to the form of the turbulent viscosity correction factor. Lewalle and Tavlarides also note that the added complexity and computation requirements of the CT model are justifiable if multiple length scales are essential to the problem such as in non-equilibrium or two-phase turbulent flows. Note that spectral RANS models provide both spatial and spectral resolution. Therefore, the distribution of turbulent viscosity must be formulated in both spectral and spatial domains to provide the needed closure to the RANS equations.

A spectral approach allows the turbulence dissipation rate transport equation used in k-ε models to be eliminated. Moreover, the detailed TKE scale information can be used to extend this model to dispersed multiphase flows. The latter potential would be impossible using multiple-time-scale models with only two or three scales since the full resolution of the TKE spectrum allows us to recognize the non-linear influence of bubbles from different size groups on the spectrum. A spectral analysis of single and two-phase DNS data in different geometries has been performed (Brown and Bolotnov, 2016) to enhance development of a more physically derived bubble source term for use in spectral cascade models.

The low-Reynolds number (i.e. wall-resolved) spectral cascade-transport model (SCTM) presented in this paper is an extension of the model the authors have developed for single and two-phase flows for the decay of isotropic turbulence (Bolotnov et al., 2008a), uniform shear flow (Bolotnov et al., 2008b), and a high-Reynolds number model for single-phase channel flow (Bolotnov et al., 2009) where wall functions were used to achieve closure near the wall of the conduit. The model presented herein resolves the turbulence in the boundary layer all the way through the laminar sub-layer, thus eliminating the need for wall function boundary conditions in the near wall TKE spectrum. The model formulation utilizes both spectral and spatial damping functions to account for the presence of the wall.

The previous model formulation (Bolotnov et al., 2009) required a boundary condition for the TKE at the smallest resolved y^+ value (typically about 30), as is often the case in the CFD modeling of turbulent flows (LAHEY et al., 1993). The previous work (Bolotnov et al., 2009) was only applied to a channel flow for a turbulent Reynolds number based on friction velocity (Re_τ) of 180. A pure inertial

subrange was not observed for such a relatively low Reynolds number and the expected -5/3 slope in the inertial subrange could not be verified. The presented work expands the model capabilities beyond decay of isotropic turbulence (Bolotnov et al., 2008a), uniform shear flows (Bolotnov et al., 2008b), and channel flow without resolving the near wall behavior (Bolotnov et al., 2009). The model concept and basic formulation can be seen in our previous publications (Bolotnov et al., 2008a,Bolotnov et al., 2008b,Bolotnov et al., 2009) and can be studied to examine these "building blocks" in the SCTM development. In the current work the turbulent boundary layer is fully resolved and therefore the need for *a priori* boundary conditions based on the law of the wall and DNS data is eliminated. The Reynolds number of the modeled flow is considerably increased and the expected -5/3 slope in the inertial subrange of the energy spectrum is confirmed. The SCTM has been implemented into the three-dimensional (3D) multiphase CFD code NPHASE-CMFD that was developed by Interphase Dynamics, LLC (2002) and the results from NPHASE-CMFD are also presented here.

The presented model is tested exclusively for channel flow as a precursor to the eventual expansion into more complex geometries (e.g. nuclear reactor sub-channels with mixing vanes and spacer grids). Extending the model to dispersed multiphase flows while maintaining the fully resolved TKE spectrum will greatly enhance multiphase flow analysis capabilities for high void fraction and polydispersed flow applications as demonstrated in Bolotnov et al. (2008a) for decay of isotropic turbulence. Resolving the turbulence all the way to the wall eliminates the need for controversial multiphase law of the wall boundary conditions that would otherwise need to be used in the previous formulation (Bolotnov et al., 2009) when extended to multiphase flows.

DNS data from single-phase turbulent channel flows for various Reynolds numbers (Del Alamo et al., 2004,del Alamo and Jimenez, 2003,Hoyas and Jimenez, 2006) has been used for model validation as well as model development and calibration. The spectral results of del Alamo et al. (2004) and Hoyas & Jiminez (2006) are used to provide a direct comparison between the SCTM and DNS. The SCTM was first evaluated using the one-dimensional (1D) partial differential equation solver FlexPDE (PDE Solutions Inc.) (www.pdesolutions.com).

2 MODEL FORMULATION

The RANS equations are solved using a turbulent viscosity determined by the SCTM equations where the Boussinesq approximation requires that the turbulent viscosity be modeled to obtain closure. In the case of the SCTM the TKE spectrum is modeled by splitting the total TKE into N wave number bins and solving separate, but coupled, transport equations for each wave number bin. Each wave number bin transport equation has similar source terms as used in typical k-ε models (JONES and LAUNDER, 1972); namely, turbulent production, dissipation, and both turbulent and viscous diffusion. A spectral transfer

term must be included to account for the energy transfers between the adjacent wave number bins. Following Lewalle & Tavlarides (1994), the general form of the single-phase version of the spectral turbulent cascade transport equation for bin-m is:

$$\frac{Dk_m}{Dt} = P_m - \varepsilon_m + D_m + T_m \tag{1}$$

where D_m, P_m, ε_m, and T_m are the diffusion, production, dissipation and transfer of the TKE in bin-m, respectively.

Previous publications pertaining to SCTM development (Bolotnov et al., 2008a,Bolotnov et al., 2008b,Bolotnov et al., 2009) have provided the procedure for determining the number of required spectral bins (N) and wave number boundaries of each bin to be used for a particular flow scenario. The presented model maintains logarithmically equal wave number spacing throughout the domain. However, to account for the wall influence, additional terms will be introduced which will significantly reduce the energy of large eddies close to the wall. It is still recommended that the spectral resolution parameter ξ be no greater than 2 (LEWALLE and TAVLARIDES, 1994).

2.1 Spectral Transfer

The spectral transfer (i.e. eddy cascade) term, T_m, models the non-linear interactions between the wave number bins. As in prior work (Bolotnov et al., 2008a), it is assumed that there is a forward spectral transfer, which represents the cascade of kinetic energy from large eddies to smaller eddies, and an inverse (i.e. backward) cascade which represents the transfer of kinetic energy in the opposite direction. The spectral transfer equation can be studied in detail in previous work (Bolotnov et al., 2009).

The DNS results of Trofimova et al. (2009), Del Alamo et al. (2004) and Hoyas & Jiminez (2006) were used to develop the directional transfer parameters for various Reynolds number (i.e., Re_τ = 180..2000) turbulent channel flows. The spectral transfer coefficients C_1 and C_2 are model parameters which quantify the directional spectral transfer rates:

$$C_1 = 16.0 - 14.8\left(1 - \exp\left(-\frac{y^+}{40.0}\right)\right)^2, \quad C_2 = 0.3167C_1 \tag{2}$$

Note that a "low-Reynolds number" type wall correction is used for the spectral transfer coefficients in the current work that approaches the spectral transfer rates (C_1 = 1.2 and C_2 = 0.38) used for the decay of isotropic turbulence (Bolotnov et al., 2008a) and uniform shear flow (Bolotnov et al., 2008b).

The spectral transfer term has been formulated in such a way as to satisfy the required constraint that the sum of all the spectral components of the transfer term does not contribute to the total TKE:

$$\sum_{m=1}^{N} T_m = 0 \tag{3}$$

2.2 Dissipation

For non-homogeneous flows there exist two different contributions to the turbulent dissipation rate (Bolotnov et al., 2010). The first component, the so-called homogeneous dissipation, results from molecular viscosity acting on the smallest eddies in homogeneous planes which are parallel to the channel walls. This dissipation component approaches zero near the wall. The other component, the inhomogeneous dissipation, is related to the shear between the homogeneous planes parallel to the wall. As can be seen in Figure 1, based on the DNS data (Bolotnov et al., 2010), this component is non-zero at the wall. A similar approach to decompose the turbulence dissipation into homogeneous and inhomogeneous components was taken by Cadiou et al. (2004). DNS data (Figure 1) (Bolotnov et al., 2010) was used to represent the inhomogeneous dissipation as those components of the dissipation tensor that are non-zero at the wall and the remaining components (those that are zero at the wall) as the homogenous dissipation.

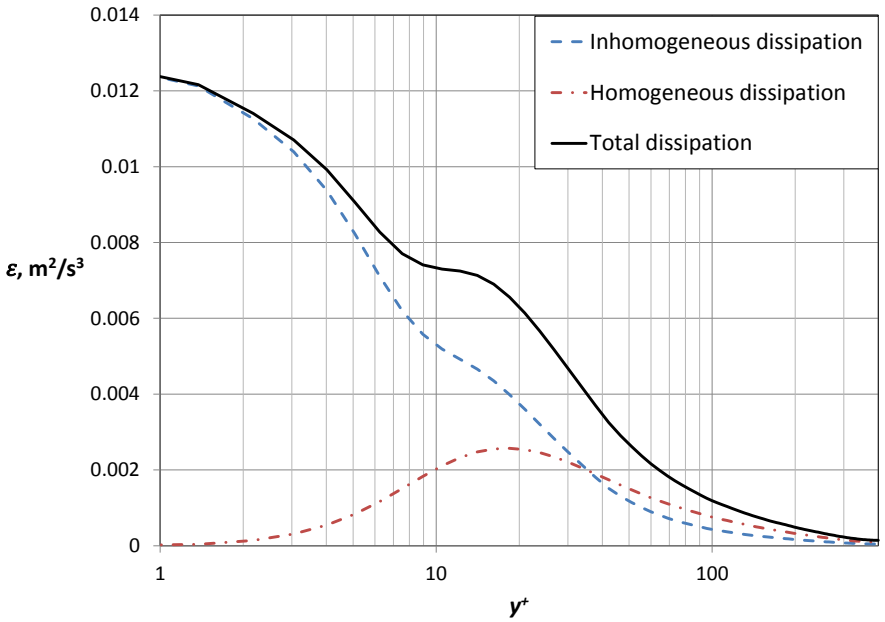

Figure 1. Turbulent dissipation components: homogeneous dissipation (dash-dot line) and inhomogeneous dissipation (dashed line). Based on the DNS results of Bolotnov et al. (2010).

As in previous work with the SCTM (Bolotnov et al., 2009), a well-known spectral formula for spectral dissipation (Cadiou et al., 2004,Pope, 2000) is used to compute the homogeneous dissipation for bin-*m* [2]:

$$\varepsilon_m^p = \int_{\kappa_{m-1}}^{\kappa_m} 2\nu\kappa^2 E(\kappa)d\kappa \cong 2\nu\frac{k_m}{\Delta\kappa_m}\left(\frac{\kappa_m^3}{3} - \frac{\kappa_{m-1}^3}{3}\right) \quad (4)$$

where the turbulent energy density function, $E(\kappa)$, has been approximated as a constant (i.e. Riemann integration) in each wave number bin interval (κ_{m-1}, κ_m).

The inhomogeneous dissipation depends on the distance from the wall (y) and has to be modeled separately for wall-bounded flow. Based on previous work (Bolotnov et al., 2010) and the analysis of the direct numerical simulation (DNS) results of Trofimova et al. (2009) the following model was developed for the inhomogeneous dissipation in wall-resolved turbulent flows:

$$\varepsilon_m^y = \left[C_{\varepsilon 1} \frac{dU}{dy} u_\tau \nu (\kappa_m - \kappa_{m-1}) + C_{\varepsilon 2} \frac{k_m}{\Delta \kappa_m} u_\tau \left(\frac{\kappa_m^2}{2} - \frac{\kappa_{m-1}^2}{2} \right) \right] \exp(-0.15 y^+) \tag{5}$$

where $C_{\varepsilon 1}$ = 0.25 and $C_{\varepsilon 2}$ = 0.05 are model constants and k is the total TKE. This model ensures that the inhomogeneous dissipation is non-zero at the wall and depends upon the local TKE. The exponential wall-correction term in Eq. (5) dictates that the inhomogeneous dissipation does not have a significant effect away from the walls, as physically expected. Although this inhomogeneous dissipation term provided good predictions of mean flow parameters when tested using the 1D PDE solver FlexPDE it required modification for the SCTM to be implemented into a 3D M-CFD code. This modification was justifiable due to the presence of the mean velocity gradient in Eq. (5). In general, sharp gradients of mean flow velocity are present particularly at the initialization of CFD simulations. These sharp gradients create unrealistically high values of the turbulence dissipation when using Eq. (5) in the SCTM and numerical convergence becomes increasingly difficult. Therefore, a new formulation for inhomogeneous dissipation was developed based on the limit of the dissipation value near a solid wall boundary as defined by Wilcox (2002). The inhomogeneous dissipation term is now:

$$\varepsilon_m^y = \frac{2.0 k_m \nu}{y^2} \exp(-0.15 y^+) \tag{6}$$

where (y) is the distance to the closest solid wall boundary. Note that Eq. (6) still contains the exponential wall-correction term but is fundamentally simpler than the original inhomogeneous formulation in Eq. (5). Finally, the total dissipation (ε) is the sum of both contributions:

$$\varepsilon = \sum_{m=1}^{N} \varepsilon_m = \sum_{m=1}^{N} \left(\varepsilon_m^p + \varepsilon_m^y \right) \tag{7}$$

2.3 Production

The spectral production of turbulence is computed using an eddy viscosity model (Hinze, 1975) so that the Reynolds stress is given by the product of the local shear rate and the spectral turbulent viscosity:

$$P_m = \nu_m^T \left(\frac{\partial U_i}{\partial x_j} + \frac{\partial U_j}{\partial x_i} \right) \frac{\partial U_i}{\partial x_j} \tag{8}$$

where ν_m^T is the turbulent viscosity of bin-m. The total turbulent viscosity that is used in the RANS equations is the sum of the bin turbulent viscosities for all of the wave number bins:

$$\nu^T = \sum_{m=1}^{N} \nu_m^T \tag{9}$$

This assures that the spectral production components sum to the proper total. For example, for stream wise flow only in the *U* direction and the *y* component normal to the wall the total turbulence production is given by Eq. (10):

$$P = \nu^T \left(\frac{dU}{dy}\right)^2 \tag{10}$$

As in the previous work (Bolotnov et al., 2009), the approach of Lewalle and Tavlarides (1994) was followed to develop a spectral turbulent viscosity for use in the analysis of homogeneous shear flows. They used Heisenberg's viscosity model (Hinze, 1975) with a spectral correction that was applied outside of the inertial subrange:

$$\nu_m^T|_{L\&T} = C_H \Delta\kappa_m \sqrt{\frac{E(\bar{\kappa}_m)}{\bar{\kappa}_m^3}} \left[E(\bar{\kappa}_m)\bar{\kappa}_m^{5/3}\varepsilon^{-2/3}\right]^{0.75} \tag{11}$$

However, since the SCTM is under-development for non-homogeneous turbulent flows a modified turbulent viscosity must be used that accounts for the presence of the wall by use of damping functions:

$$\nu_m^T = f_\mu f_y f_s \nu_m^T|_{L\&T} = C_H f_\mu f_y f_s \Delta\kappa_m \sqrt{\frac{E(\bar{\kappa}_m)}{\bar{\kappa}_m^3}} \left[E(\bar{\kappa}_m)\bar{\kappa}_m^{5/3}\varepsilon^{-2/3}\right]^{0.75} \tag{12}$$

where C_H = 0.40 is a model constant. The spectral wall function, f_y, damps the larger eddies close to the wall:

$$f_y = \left[1.0 - \exp\left(C_y \bar{\kappa}_m y\right)\right]^{N_y} \tag{13}$$

and $f_\mu$is a Chien (1982) type "low-Reynolds number" near-wall correction which is frequently used in k-ε models:

$$f_\mu = 1.0 - \exp\left(C_\mu y^+\right) \tag{14}$$

and f_s is a spectral damping function that controls the energy of the largest eddies in the flow:

$$f_s = 1.0 - \exp\left(C_s \frac{\bar{\kappa}_m}{\kappa_N}\right) \tag{15}$$

The damping functions in Eqs. (13) – (15) contain the majority of SCTM constants that must be tuned for model performance. A comparison of the values used for the initial 1D FlexPDE testing and the current model values for use in the 3D M-CFD code are shown in Table 1. SCTM constants required some adjustment after the implementation of the new inhomogeneous dissipation term.

Table 1. SCTM constants.

Model Constant	FlexPDE	NPHASE-CMFD
C_y	-1.6	-1.6
N_y	0.5	0.25
C_μ	$-7.38 \times 10^{-3} \exp(-8.53 \times 10^{-4} Re_\tau)$	-0.007
C_s	-175.0	-125.0

2.4 Diffusion

The spectral turbulent and viscous diffusion term is modeled much like in the previous work (Bolotnov et al., 2009):

$$D_m = \nabla \cdot \left(\left[\nu + \frac{\nu_T}{\sigma_k} \right] \nabla k_m \right) \tag{16}$$

where σ_k= 0.5.

2.5 Relationship of the SCTM to Two-Equation k-ε Type Models

It is interesting to sum the spectral cascade-transport turbulence model equations (1) over all bins. Since, as can be seen in (3), the spectral transfer term does not contribute to the overall TKE the source term components on the right hand side of the sum of (1) are the same as in standard single-phase k-ε models:

$$\frac{Dk}{Dt} = P - \varepsilon + D \tag{17}$$

where k is the overall TKE, P is the total production of TKE, ν_T is defined in (9), ε is the turbulent dissipation rate defined in (7), and $\sum_{m=1}^{N} D_m$ is the total viscous/turbulent diffusion term. The exact expression for some of these source terms do not precisely correspond to the empirical results used in k-ε TKE transport model, rather the expressions for ε and ν_T quantify complicated spectral integrations. However, the spectral cascade-transport turbulence model does not require the use of a transport equation for turbulent dissipation rate as a k-ε model does but is capable of good predictions of the DNS results while also providing spectral information.

3 NUMERICAL TOOLS

3.1 FlexPDE

The 1D SCTM formulation was first implemented into the partial differential equation solver FlexPDE (PDE Solutions Inc.) (www.pdesolutions.com) to numerically evaluate the model and assess its performance for fully-developed single-phase channel flow. FlexPDE software converts a user defined system of partial differential equations into a finite element model and then chooses an appropriate numerical solution scheme (PDE Solutions Inc.). Although FlexPDE has dynamic time-stepping

capabilities, a constant time step of 1.0 was used for each of the presented cases for improved convergence of the model due to its highly non-linear nature. Spatial mesh resolution across the channel width was varied using Eq. (18) to accurately resolve the wall boundary layer, such that a finer mesh was employed closer to the wall and a coarser mesh utilized closer to the channel center line. Validation of the 1D SCTM was performed with FlexPDE so that the primary focus could be on improving the flow physics modeling by taking advantage of a robust numerical treatment to solve the equations, to use the in-situ visualization of FlexPDE for simulation control and improved model development efficiency, and to pose the equations in a natural scripting language.

$$dy = 0.85\left[1.4 + 25.0\left(\tan^{-1}\left\{y\pi - \frac{\pi}{2}\right\}\right)\frac{\nu}{u_\tau}\right] \tag{18}$$

3.2 NPHASE-CMFD

Developing the SCTM for use by a 3D M-CFD code is important for extending the model to multidimensional problems, taking advantage of high quality meshing software for complex nuclear geometries, including the energy equation and heat transfer terms, and taking advantage of the inherent multiphase and multiprocessor capabilities of powerful CFD packages. The NPHASE-CMFD code was developed by Interphase Dynamics, LLC and was chosen for 3D implementation of the SCTM because its powerful multiphase capabilities align well with the two-phase model development plan. NPHASE-CMFD was developed as a reliable solver for multiphase flows with the ability to use unstructured grids of arbitrary element type, model an arbitrary number of fluid components, handle user-implemented multiphase closure modeling, and utilize parallel processing using the MPI protocol (Interphase Dynamics, 2002). NPHASE-CMFD can also model an arbitrary number of chemical species, N_s, mixed in a chosen field by use of N_s species transport equations of the form (Interphase Dynamics, 2002):

$$\frac{\partial(\alpha_j\rho_j Y_m)}{\partial t} + \nabla\cdot\alpha_j\rho_j\bar{v}_j Y_m = J_m + S_m\ ,\quad J_m = \nabla\cdot\left[\alpha_j\left(\frac{\mu_j}{\sigma_s} + \frac{\mu_j^T}{\sigma_s^T}\right)\nabla Y_m\right] \tag{19}$$

where subscript-j indicates the advecting fluid-j of the species mass fraction-Y_s. Note that the general scalar transport equation (19) for the species mass fraction, Y_m, is analogous to the SCTM TKE transport equation (1) for a particular bin TKE, k_m. The capability of NPHASE-CMFD to solve an arbitrary number of scalar species transport equations has been repurposed for the SCTM. Rather than solving for the species mass fraction, the SCTM source terms have been implemented the into the species transport equations such that they now solve for the TKE in each bin. NPHASE-CMFD handles the viscous/turbulent diffusion term as J_s and the remaining SCTM source terms can be user-implemented into the right hand side source term S_m:

$$S_m = P_m + \varepsilon_m^p + \varepsilon_m^y + T_m \tag{20}$$

Figure 2 shows the iteration process for the chemical species mass fraction transport equations repurposed for the SCTM. Note that NPHASE-CMFD is not open-source and the code can only be accessed by the user through specific user functions. The user routines used to implement the SCTM are also denoted in Figure 2. The turbulent viscosity is updated using the SCTM and then fed into the RANS equations. The normal code framework for NPHASE-CMFD to solve the momentum and mass equations (and energy if requested) is not altered. Since NPHASE-CMFD has the ability to solve N_s species transport equations, the number of bins can easily be user-controlled.

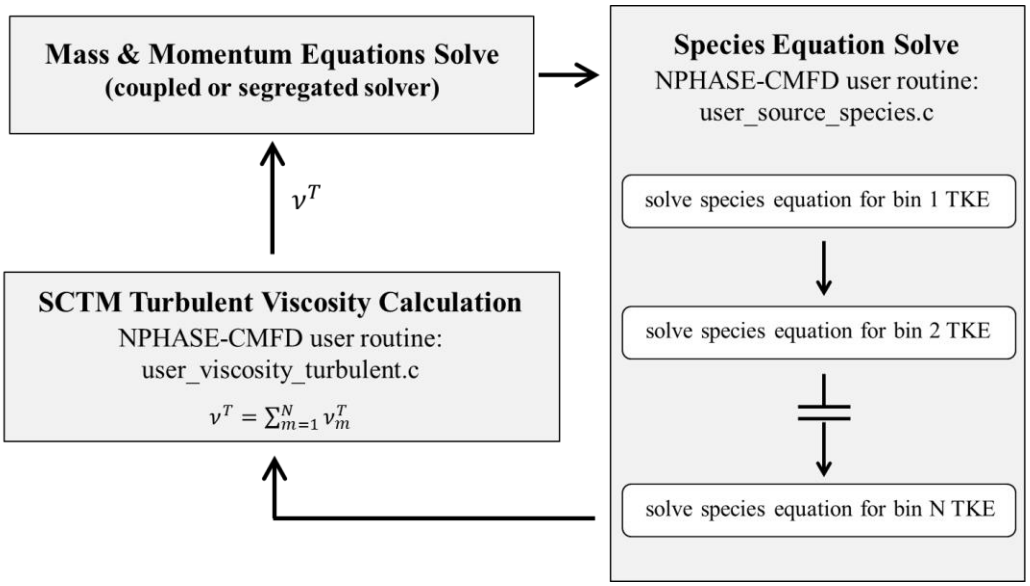

Figure 2. NPHASE-CMFD iteration process for the repurposed chemical species equations.

4 RESULTS

Results for the SCTM with the inhomogeneous dissipation term defined by Eq. (5) will first be presented followed by results for the SCTM implemented into the NPHASE-CMFD code with inhomogeneous dissipation defined by Eq. (6). The model constants used for both FlexPDE and NPHASE-CMFD are provided in Table 1. The FlexPDE results will be provided for reference and comparison in the presentation of the NPHASE-CMFD results.

4.1 1D FlexPDE

FlexPDE was used for calibration and development of the SCTM with DNS data for three different Reynolds number cases of turbulent channel flow. The DNS data is examined in comparison to the SCTM as a 1D slice across one-half of the channel width in terms of distance from the wall. The DNS data (Re_τ= 2000) of Hoyas and Jiminez (2006) and (Re_τ= 950) del Alamo et al. (2004) allow for validation of not only mean flow parameters, but for model validation of the performance in the spectral domain as well since the DNS information in the spectral domain is available. The SCTM performance

has also been assessed for lower Reynolds number turbulent channel flow (Re_τ= 550) using the DNS data of del Alamo and Jiminez (2003). Table 2 lists the values of model parameters for all of the considered cases.

SCTM results from 1D FlexPDE will be shown for the 3 considered Reynolds numbers (Re_τ = 550, Re_τ = 950, Re_τ = 2000) in comparison to DNS data as well as the low-Reynolds number Chien k-ε model (1982). Overall, predictions of the SCTM are on par with the Chien k-ε model and provide good predictions of the DNS data while also resolving the TKE spectrum.

Table 2. SCTM parameters for the channel flow computations.

Parameter description	**Notation**	$\boldsymbol{Re_\tau}$**=550**	$\boldsymbol{Re_\tau}$**=950**	$\boldsymbol{Re_\tau}$**=2000**	**Units**
Friction velocity	u_τ	0.04890	0.04539	0.04130	m/s
Kinematic viscosity	ν	8.945e-5	4.859e-5	2.062e-5	m^2/s
Domain left boundary	y_0^+	0.0	0.0	0.0	-
Domain right boundary	y_1^+	546.70	934.13	2003.15	-
Number of cascade bins	N	18	5 - 22	18	-
Spectral resolution parameter	ξ	1.3921	3.361 - 1.317	1.4553	-
Spatial mesh resolution	Δy^+	0.38 – 1.8	0.38 – 3.1	0.34 – 6.7	-
Left boundary of wave number range (largest liquid eddies)	κ_0	1.000	1.333	1.333	1/m
Right boundary of wave number range (smallest liquid eddies)	κ_N	385.7	571.7	1144.0	1/m

4.1.1 $\boldsymbol{Re_\tau}$ = 2000

The highest Reynolds number case will be discussed first. As can be seen in Figure 3 the SCTM demonstrates good prediction of the mean velocity profile and reasonable agreement for the total TKE profile. Note that a non-dimensional TKE scale $\left(k^+ = {}^{k}/_{u_{\tau^2}}\right)$ was used on the right vertical axis of the plot. Comparisons with the Chien k-ε model show that although TKE is over-predicted by the SCTM, mean velocity is likewise over-predicted by the Chien k-ε.

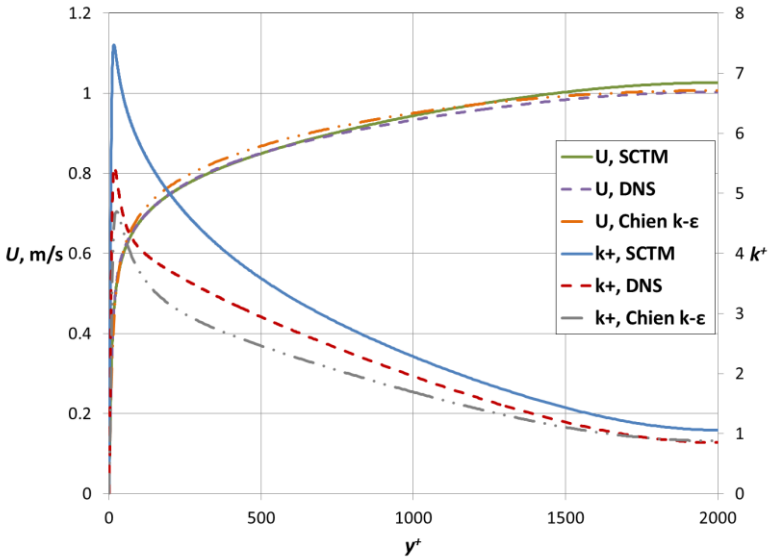

Figure 3. Mean velocity and TKE profiles obtained by the SCTM using eighteen (N = 18) wave number bins (solid lines) compared to DNS results (Re_τ= 2000) of Hoyas and Jiminez (2006) (dashed lines) and the Chien k-ε model (1982) (dashed dot dot lines).

Figure 4 compares SCTM results with the well-known law of the wall:

$$U^+ = \frac{1}{\kappa_0} \ln y^+ + B \tag{21}$$

where κ_0= 0.39 and B = 4.7. The law of the wall indicates that the stream wise velocity in the flow varies logarithmically with distance from the wall surface (WILCOX, 2002). For the SCTM, excellent agreement is shown in the region of applicability of the law of the wall as well as with the DNS data all the way to the wall. The SCTM provides better prediction of the mean velocity than the Chien k-ε model. Unlike in previous spectral cascade-transport models of channel flow (Bolotnov et al., 2009), a wall function boundary condition is not needed to achieve closure.

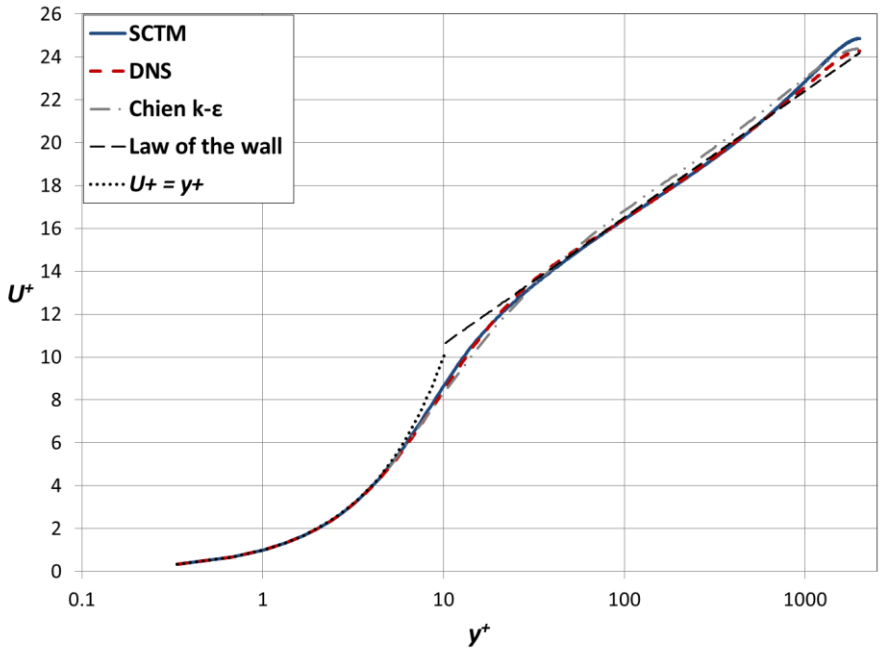

Figure 4. Mean velocity profile of the SCTM using eighteen (N = 18, Re_τ= 2000) wave number bins (blue solid line) compared to DNS results of Hoyas and Jiminez (2006) (red dashed line), the Chien k-ε model (1982) (grey dashed dot dot line), the law of the wall, and $U^+ = y^+$ in the very near wall region.

Spectral energy results can be presented as TKE spectrum at various y^+ locations. Figure 5 compares eighteen bin SCTM energy spectrum predictions at four different y^+ locations (y^+= 2000, y^+= 1200, y^+= 400, y^+= 40) with DNS data (Bolotnov et al., 2010) and the well-known -5/3 energy spectrum slope for single-phase turbulent flows. Near the channel center line (Figure 5(a)) and through the bulk turbulence region of the flow (Figure 5(b), (c)), excellent agreement is observed between the SCTM and the DNS data. However, the model fails to predict the change in energy spectrum slope near the wall (Figure 5(d)) where it instead preserves the theoretical -5/3 slope of the inertial subrange. This could be due to slight under-predictions of viscous diffusion and dissipation close to the wall, which will be discussed in accordance with Figure 7(d). Applying the SCTM to much higher Reynolds number than were previously examined by Bolotnov et al. (2009) for channel flow without resolving the near-wall boundary layer has shown that the model predicts the theoretical -5/3 slope of the inertial subrange. At this particular Reynolds number (Re_τ= 2000), inner and outer scale separation are large enough to observe the inertial subrange and validate model behavior.

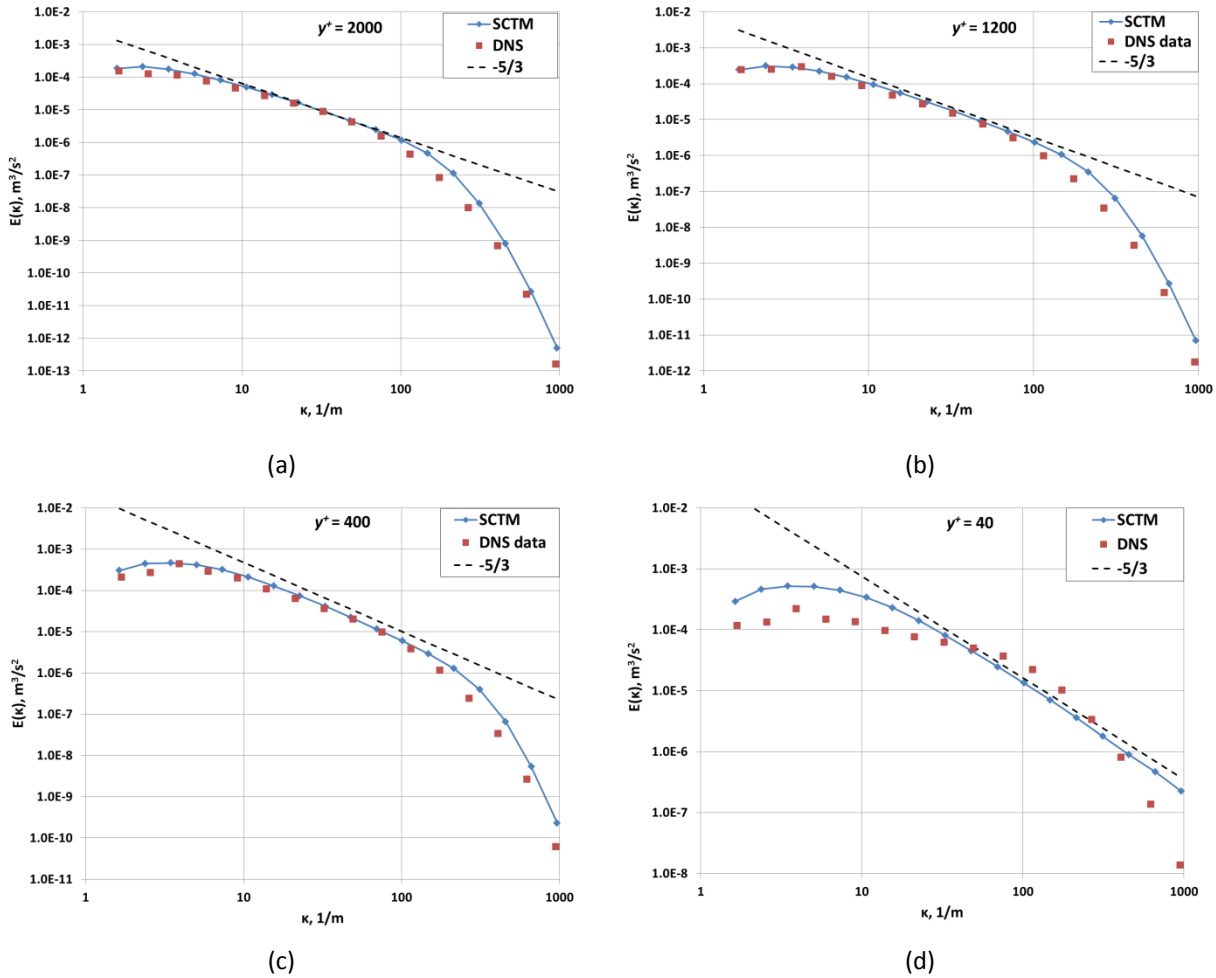

Figure 5. SCTM (N = 18, Re_τ= 2000) prediction of the TKE spectrum at four different distances from the wall: (a) y^+= 2000, (b) y^+= 1200, (c) y^+= 400, and (d) y^+= 40 (blue solid line with diamonds) in comparison to DNS data spectrum (red squares) and -5/3 slope (dashed line).

The spectral energy results can also be represented as contours in the spectral and spatial domains (Figure 6). The peak of TKE is clearly shown in the small wave number region and further from the wall since the largest liquid eddies in the flow cannot be present close to the wall. Specifically, the TKE peak is mostly concentrated within bin 3 at a y^+ value slightly less than 100. Observing Figure 5(b)-(d) the higher TKE values in bin 3 are present within the DNS data as well. The smallest liquid eddies in the higher wave number ranges are expected close to the wall where viscous effects are substantial. The contour plot approach is a convenient way to represent the behavior of the turbulence in both physical and spectral spaces and this approach was used in the spectral analysis of DNS data by Bolotnov et al. (2010).

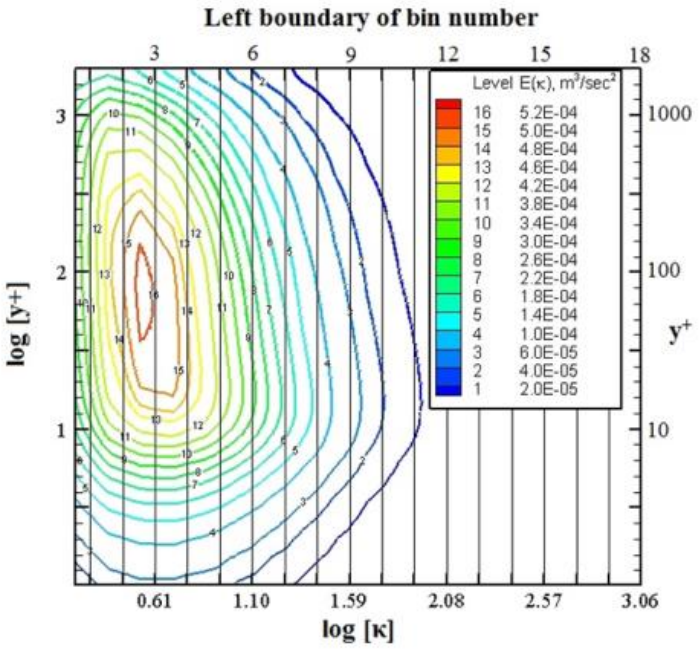

Figure 6. SCTM predictions of the TKE contour levels in the spectral and spatial domains. The vertical gridlines represent spectral bins for N = 18, Re_τ= 2000 case and bin numbers are denoted on the top axis of the plot. Contours are plotted based on the logarithmic wave number and logarithmic y^+ scales.

Examining SCTM source terms (i.e. the right hand side terms of the single-phase cascade-transport equation (1)) in both the spatial and spectral domain indicates that the model behaves as expected in terms of energy production at the lowest wave number bins, energy transfer through the inertial subrange, and the eventual dissipation of the smallest eddies at the highest wave number bins. Figure 7(a) shows the SCTM source term balance for bin #5. Eddies in this bin are sized approximately as one-sixth of the channel half width (Table 3). Recalling the peak of energy production from the contour plot in Figure 6 it is consistent that eddies in this bin receive energy predominately through the production term (dashed blue line) while energy is removed by the spectral transfer term (red dashed dot dot line) through the energy cascade process. Both the viscous and turbulent diffusion (teal dashed dot line and orange dotted line) terms are considerable in bin #5, where viscous effects are present close to the wall (i.e. y^+ less than about 10) and the change in turbulent diffusion sign occurs to keep the source term balance equal to zero when viscous effects are no longer present. Note that dissipation effects are negligible for eddies of this size.

However, for bin #11 (Figure 7(b)) the source terms are distributed much differently. In this bin, eddies are sized as approximately one-fifty second of the channel half width. Noting the location of bin #11 in Figure 5, this bin resides at the transitional point between the -5/3 slope of the inertial subrange and the steeper slope of the dissipation range. Here, effects of each of the source terms are evident. Due to the log-scale nature of the bin boundaries these eddies are still dominated by the production term although

dissipation effects are becoming evident. Figure 7(b) also shows fully-developed steady state model predictions for bin #11 since the sum of all source terms is essentially zero.

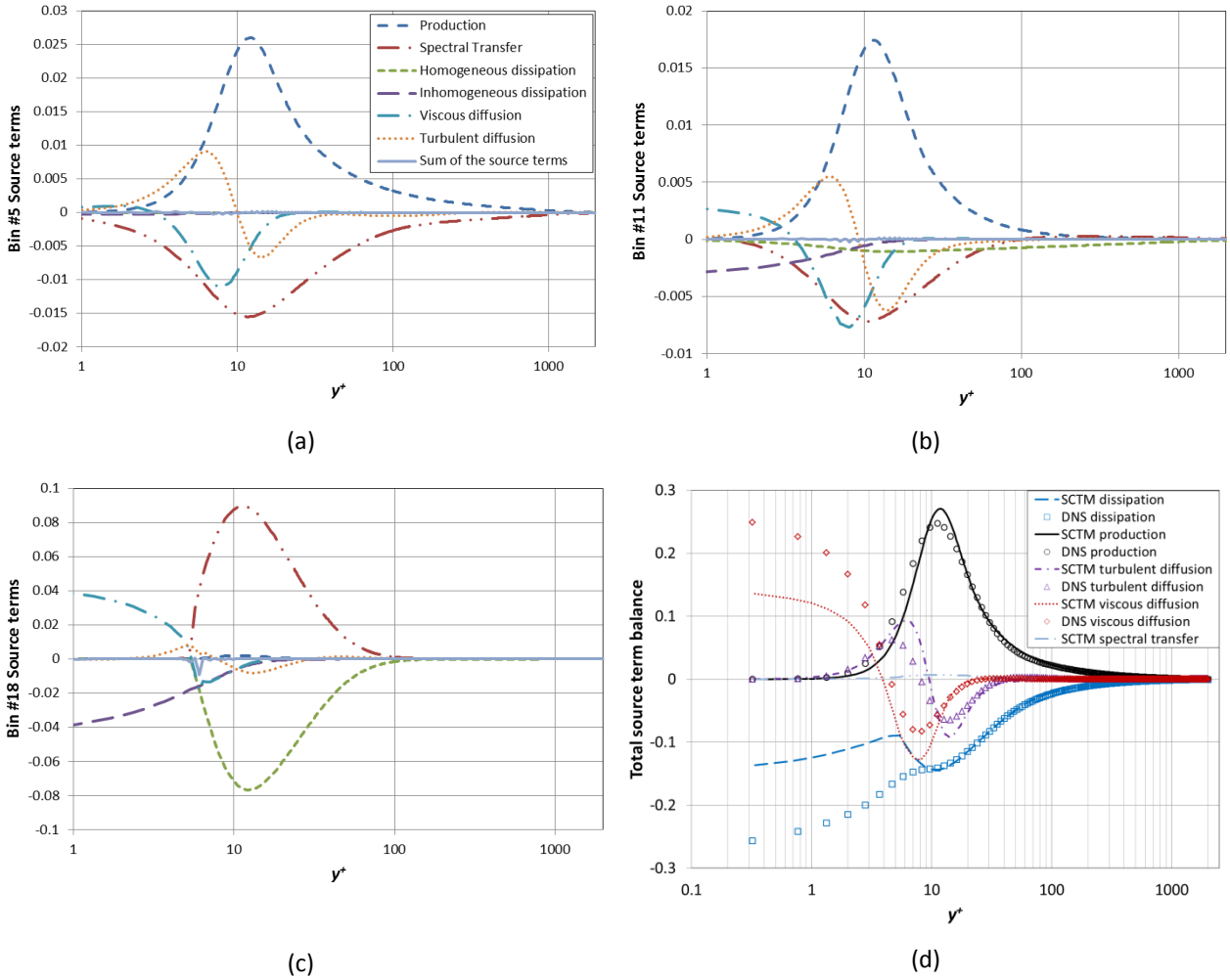

Figure 7. (a) - (c): SCTM results for the source term distribution of the cascade-transport equation for bin numbers 5, 11, and 18, respectively (N = 18, Re_τ= 2000). (d): The total source term balance of the SCTM in comparison to the DNS results of Hoyas and Jiminez (2006).

Figure 7(c) shows the SCTM source term distribution for bin #18, or the smallest eddies present in the flow. In this bin, the spectral transfer term transports energy through the left wave number boundary of the bin as energy cascades down from larger eddies. The viscous diffusion term also provides energy in this bin. The homogeneous and inhomogeneous dissipation terms (dashed green line and long-dashed purple line) dominate in removing TKE from the turbulent eddies.

The total source term balance for the SCTM can be obtained by summing the spectral source terms for each bin. The total source term balance for the SCTM (N = 18, Re_τ = 2000) in comparison to the DNS data of Hoyas and Jiminez (2006) is shown in Figure 7(d). The SCTM predicts these terms quite well, most notably in predicting spatial peak locations, although there is some disagreement in the

dissipation and viscous diffusion terms close to the wall. As aforementioned, this disagreement may account for the SCTM failing to predict the slope change of the TKE spectrum close to the wall in Figure 5(d). Also, recall that the inhomogeneous dissipation used for FlexPDE (Eq. (5)) has been updated for use in the 3D M-CFD code and, as will be shown, the new term (Eq. (6)) provides a better prediction of the DNS dissipation shape. The SCTM spectral transfer term summed over the spectral space is shown in Figure 7(d) as well and the term essentially sums to zero.

Table 3. SCTM wave number boundaries for N = 18, Re_τ= 2000 case and the approximate average eddy size in each spectral bin based on the channel half width (δ).

Spectral bin number	**Left boundary wave number, 1/m**	**Right boundary wave number, 1/m**	**Approximate average eddy size**
1	1.333	1.940	4δ/5
2	1.940	2.824	δ/2
3	2.824	4.110	δ/3
4	4.110	5.982	δ/4
5	5.982	8.705	δ/6
6	8.705	12.67	δ/8
7	12.67	18.43	δ/11
8	18.43	26.83	δ/17
9	26.83	39.05	δ/25
10	39.05	56.83	δ/36
11	56.83	82.72	δ/52
12	82.72	120.3	δ/76
13	120.3	175.2	δ/110
14	175.2	254.9	δ/161
15	254.9	371.1	δ/235
16	371.1	540.1	δ/342
17	540.1	786.0	δ/497
18	786.0	1144	δ/724

Figure 8 shows the non-dimensionalized turbulent viscosity prediction of the SCTM (the sum of the bin turbulent viscosities) in comparison to DNS data and the Chien k-ε model. The DNS turbulent viscosity was evaluated using (Bolotnov et al., 2009):

$$\nu_T = \frac{\langle u'v' \rangle}{\frac{dU}{dy}} \tag{22}$$

Excellent agreement is observed close to the wall with acceptable agreement for the rest of the flow. Note that the peak loaction of turbulent viscosity is well predicted by the SCTM and center line discrepancies are observed for both the SCTM and Chien k-ε. It is important to note that the centerline behavior of the estimated turbulent viscosity has limited influence on model predictive capabilities since the relatively flat velocity profile results in small turbulent production and diffusion. On the other hand, the DNS estimates provided for comparison also have larger uncertainty close to the centerline since this artificial quantity (turbulent viscosity) is computed using the ratio of DNS-estimated turbulent shear stress ($\langle u'v' \rangle$)

over DNS-estimated velocity gradient (dU/dy). At the centerline both those quantities are expected to be zero – so turbulent viscosity is not defined using this method. As one approaches the centerline location the uncertainty grows. These two observations explain why having a disagreement between the model prediction and DNS estimates away from the wall (where velocity gradients/shear stresses are small) does not necessarily result in poor model performance (as seen for both Chien k-ε and SCTM).

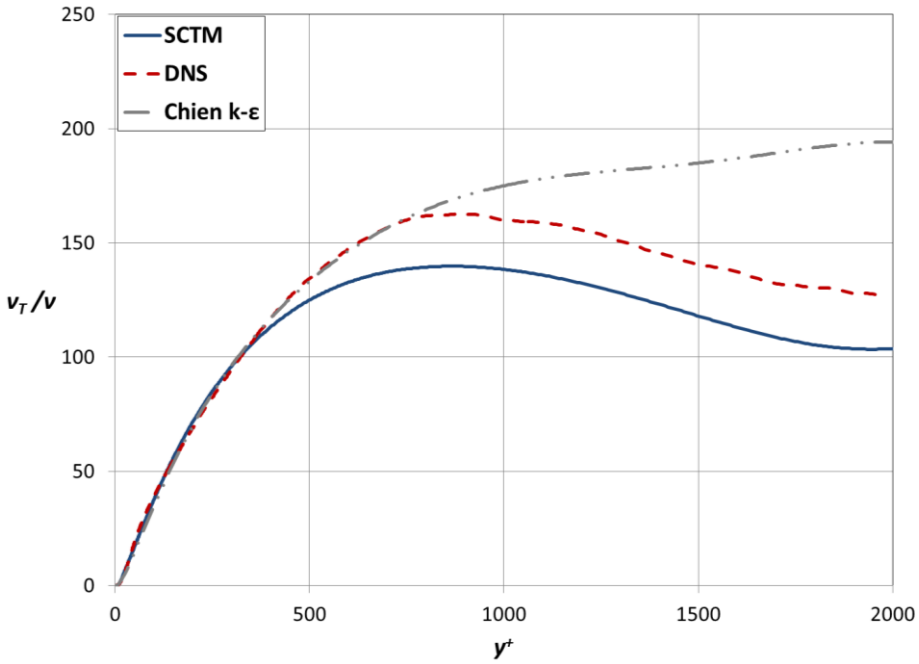

Figure 8. Non-dimensional turbulent viscosity distribution of the SCTM (N = 18, Re_τ= 2000; solid blue line) compared with DNS results of Hoyas and Jiminez (2006) (dashed red line) and the Chien k-ε model (1982) (grey dashed dot dot line).

4.1.2 Re_τ = 950

SCTM predictions for Re_τ= 950 were also performed and compared with DNS data (Del Alamo et al., 2004) and the Chien k-ε model (1982). Note that for each considered Reynolds number the model formulation remains the same as previously presented while the wave number ranges (Table 2) are different based on the requirements of the SCTM. A spectral resolution study was also performed for this particular case at Re_τ= 950 to ensure that model accuracy does not significantly degrade even when fewer wave number bins are used.

Figure 9(a) shows the mean velocity and TKE profiles calculated by the SCTM in comparison to the DNS data and Chien k-ε model. These mean flow parameters are predicted quite well. Particularly, the SCTM better predicts the mean velocity behavior than the over-prediction of the Chien k-ε model. However, the SCTM does over-predict the TKE profile further from the wall. The SCTM performs similarly to the Chien k-ε model for the turbulent viscosity (Figure 9(b)).

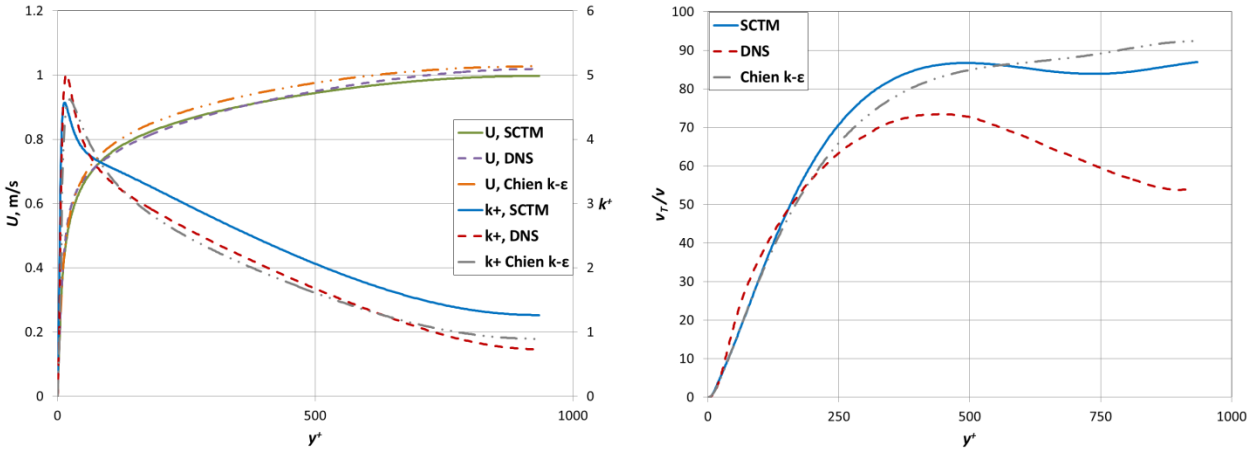

Figure 9. Mean velocity and TKE profiles (a) as well as turbulent viscosity profile (b) obtained by the SCTM (N = 18, Re_τ = 950) in comparison to the DNS data of del Alamo et al. (2004) and the Chien k-ε model (1982).

Figure 10 shows how the SCTM mean velocity (N = 18, Re_τ= 950) compares to the well-known law of the wall (Eq (21)). The SCTM predicts the law of the wall and the DNS data quite well, notably achieving the flat velocity profile in the logarithmic region of applicability and well-predicting the DNS data in the very near wall region.

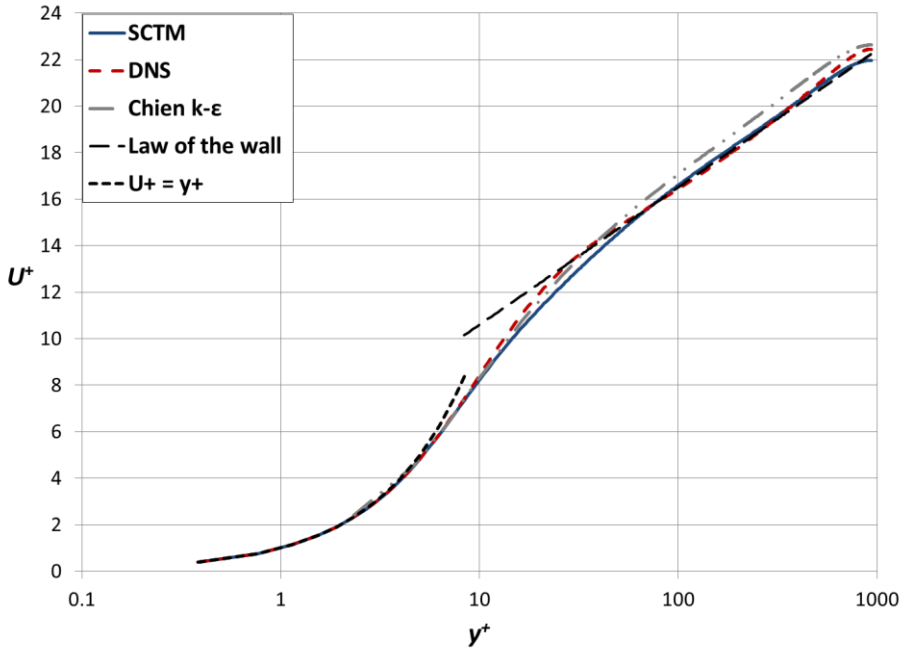

Figure 10. Mean velocity profile of the SCTM using eighteen (N = 18, Re_τ= 950) wave number bins (blue solid line) compared to DNS results of del Alamo et al. (2004) (red dashed line), the Chien k-ε model (1982) (grey dashed dot dot line), the law of the wall, and $U^+ = y^+$ in the very near wall region.

Figure 11 shows the total source term balance (the sum over all wave numbers) for the SCTM in comparison with the DNS results of del Alamo et al. (2004) for the eighteen bin Re_τ= 950 case. As with the Re_τ= 2000 case (Figure 7(d)), good agreement between the SCTM and DNS data is observed with only some notable discrepancy in the dissipation and viscous diffusion estimations close to the wall.

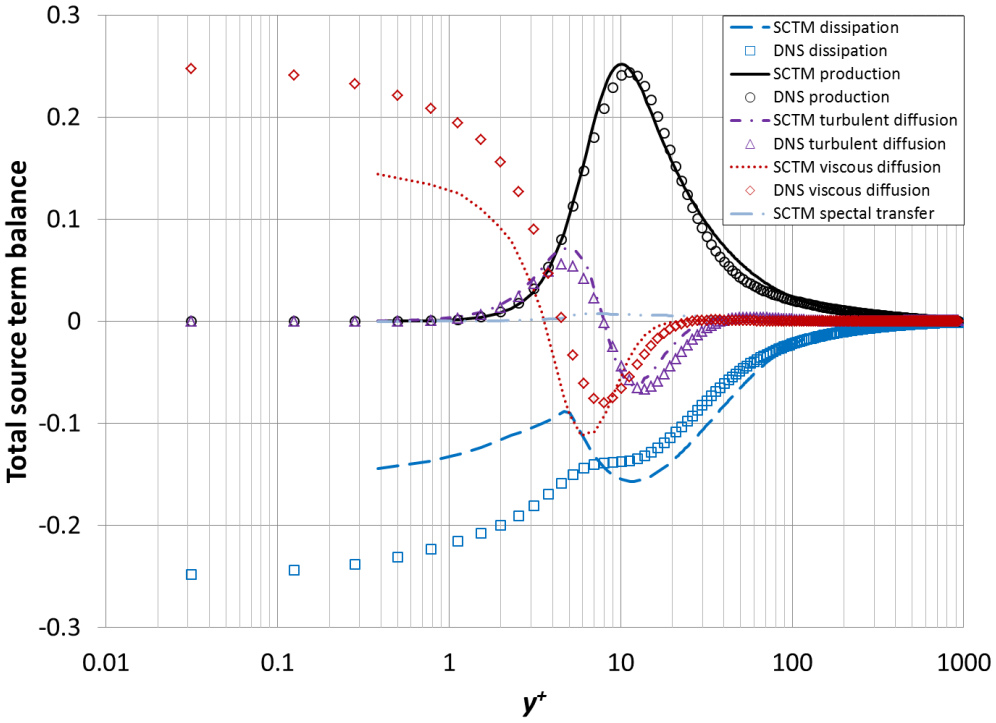

Figure 11. Total source term balance for the SCTM (N = 18, Re_τ= 950) in comparison to the DNS results of del Alamo et al. (2004).

4.1.2.1 Spectral Resolution Study

A spectral resolution study was performed for the Re_τ= 950 case where results for 5, 8, 14, 18, and 22 wave number bins were compared to gauge model performance. The spectral resolution parameter for the different number of wave number bins can be seen in Table 4. Clearly, the N = 5 and N = 8 simulations have spectral resolution parameters larger than the suggested maximum value of 2 but, as will be shown, acceptable model predictions are still possible. Figure 12 displays how turbulent viscosity behaves for the differing number of wave number bins. The N = 5 simulation does show some slightly under-predicted results in comparison to the N = 18 case. However, expected model behavior of convergence to some final solution as the number of bins is increased is observed. Behavior of the remaining mean flow parameters (i.e. mean velocity and TKE) is similar.

Table 4. Spectral resolution (ξ) values for each of the considered number of bins in the spectral resolution study.

Number of Bins	Spectral Resolution (ξ)
5	3.361
8	2.133
14	1.542
18	1.400
22	1.317

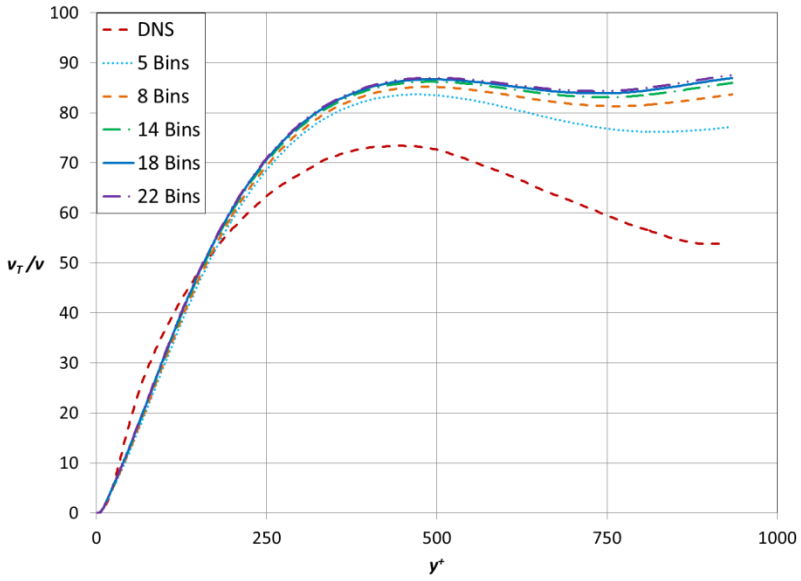

Figure 12. SCTM turbulent viscosity (Re_τ= 950) with N = 5 (blue dotted line), N = 8 (orange dashed line), N = 14 (green dashed dot line), N = 18 (solid blue line), and N = 22 (purple dashed dot dot line) wave number bins in comparison to the DNS results of del Alamo et al. (2004).

The TKE spectrum is shown for all of the considered bin numbers in the spectral resolution study at y^+ locations of 930 and 40 in Figure 13 and Figure 14, respectively. Good agreement with the DNS data is observed in the bulk turbulence region away from the wall (y^+= 930) as well as expected model behavior for different wave number resolutions; namely the higher resolutions (N = 14, N = 18, N = 22) are able to better predict changes in the slope of the energy spectrum than the lower bin number resolution cases. However, the model is still able to correctly predict the -5/3 slope in the inertial subrange and the changes in energy spectrum behavior even for the very low bin number resolutions of N = 5 and N = 8. Although the smallest allowable spectral resolution for the SCTM has been stated as 2 the spectral resolution study has shown that the SCTM is robust since minimal changes are observed even for spectral resolution as high as 3.361 (N = 5). The TKE spectrum in the near wall region (Figure 14) fails to predict the change in slope at the transition from the inertial subrange to the dissipation region much like the behavior observed in the Re_τ= 2000 case. Again, this may be due to under-predictions of dissipation and

viscous diffusion near the wall. Behavior of the total source term balance was similar for all of the different number of bins considered in the spectral resolution study.

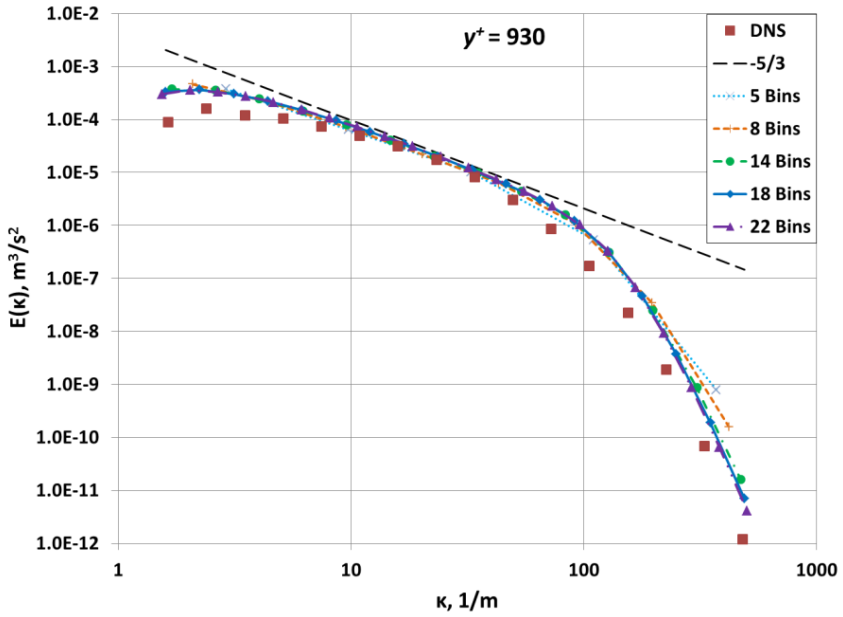

Figure 13. SCTM (Re_τ= 950) predictions of the TKE spectrum at y^+= 930 for 5 (blue "X" symbols), 8 (orange "+" symbols), 14 (green circles), 18 (blue diamonds), and 22 (purple triangles) wave number bins compared to DNS spectrum (red squares) and -5/3 slope (black dashed line).

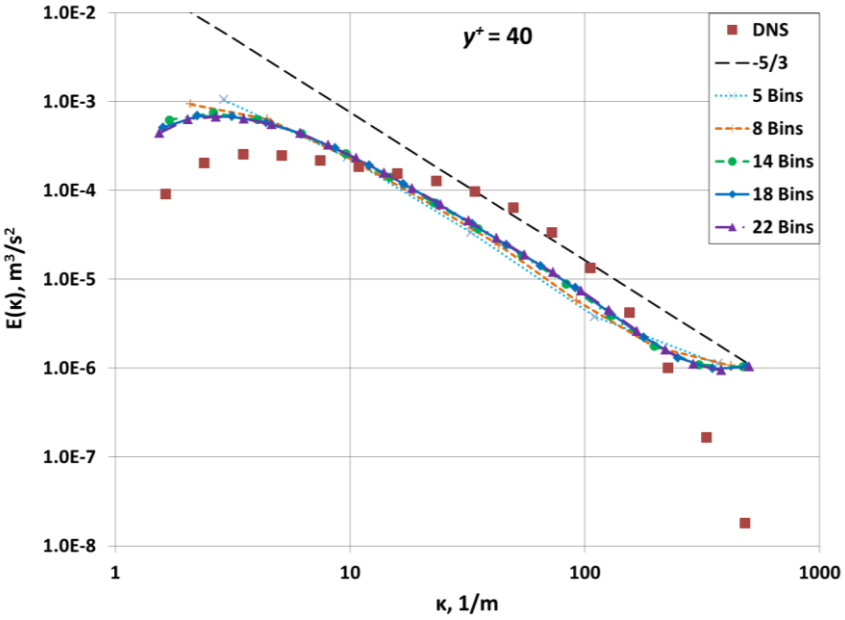

Figure 14. SCTM (Re_τ= 950) predictions of the TKE spectrum at y^+= 40 for 5 (blue "X" symbols), 8 (orange "+" symbols), 14 (green circles), 18 (blue diamonds), and 22 (purple triangles) wave number bins compared to DNS spectrum (red squares) and -5/3 slope (black dashed line).

4.1.3 Re_τ = 550

Figure 15 presents a comparison of SCTM (N = 18, Re_τ= 550) mean flow predictions with the DNS data of del Alamo and Jiminez (2003) and the Chien k-ε model (1982) for the lowest considered Reynolds number used for model calibration and validation. Decent agreement is shown between the SCTM mean velocity and DNS data while acceptable agreement is observed with the TKE magnitude and location. The Chien k-ε model again over-predicts mean velocity in comparison to the SCTM and DNS results. The SCTM missed the prediction of the turbulent viscosity (Figure 15(b)) peak. However, the Chien k-ε model predictions are no better than the SCTM and earlier discussion has been given concerning possible reasons for observed disagreement between the DNS results and models.

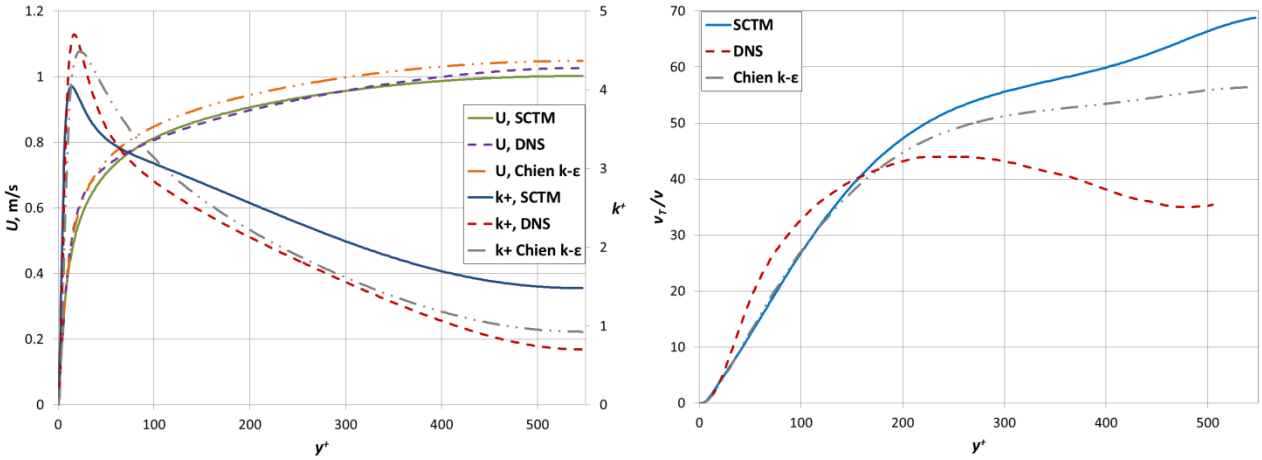

Figure 15. Mean velocity and TKE profiles (a) as well as turbulent viscosity profile (b) obtained by the SCTM (N = 18, Re_τ= 550) in comparison to the DNS data of del Alamo and Jiminez (2003) and the Chien k-ε model (1982).

Predictions of the law of the wall and overall source term balance in comparison to DNS data were similar to the results shown for the Re_τ= 2000 and Re_τ= 950 cases. The TKE spectrum comparison with the theoretical -5/3 slope of the inertial subrange and the overall spectrum shapes are consistent with expectations. At this lower Reynolds number the inner and outer scale separation is reduced but the SCTM can still be validated by the -5/3 slope in the inertial subrange. TKE spectrum results close to the wall for Re_τ= 550 are consistent with results for previous Reynolds numbers and fail to capture the change in slope from the inertial subrange to the dissipation range close to the wall.

4.2 NPHASE-CMFD

The plane channel flow geometry predicted with the SCTM using FlexPDE is an excellent starting point for testing of the SCTM in NPHASE-CMFD. These tests are the next “building blocks” in developing the SCTM to become a viable turbulence closure option for prediction of multiphase flow in complex nuclear reactor relevant geometries. Preliminary testing was performed that compared SCTM

predictions of decay of isotropic turbulence to experimental results. Both the spatial and spectral turbulence decay profiles were in excellent agreement with experimental data; providing confidence that the repurposing of the chemical species equations is an acceptable method for solution of the SCTM TKE transport equations in NPHASE-CMFD. To perform the turbulent channel flow simulations all of the TKE source terms must be implemented into NPHASE-CMFD (Eq. (20)).

Recall that a modified inhomogeneous dissipation term (Eq. (6)) was implemented in NPHASE-CMFD and further discussion is provided here to justify the change that required some additional tuning of model parameters. Both model performance and numerical convergence are exceedingly important in complex turbulence model development, particularly for highly non-linear models such as the SCTM. The original formulation for inhomogeneous dissipation (Eq. (5)) contained the derivative of mean velocity. This caused numerical issues for predominately two reasons: (i) in CFD calculations the mean velocity on the inflow is generally prescribed as a constant across the manifold which leads to high values of the gradient early in the simulation before fully-developed flow conditions; (ii) NPHASE-CMFD uses the *production destruction clip ratio* (Interphase Dynamics, 2002), or the ratio of turbulent production to turbulent dissipation, to limit the shear induced turbulence during early iterations and this approach should be used with the SCTM as well. Therefore, if the turbulent dissipation contains the mean flow gradient then limiting turbulent production based on turbulent dissipation rate becomes non-sensible and the calculations become increasingly numerically stiff. As shown previously, SCTM predictions with 1D FlexPDE for the overall energy budget (Figure 7(d) and Figure 11) under-predicted the dissipation close to the wall that is controlled by inhomogeneous dissipation. After careful deliberation the most practical plan of action was then to improve both model behavior and numerical convergence by implementing the modified inhomogeneous dissipation term (Eq. (6)). As stated previously, this required some tuning of model parameters and those changes are reflected in Table 1. Note that for all of the NPHASE-CMFD results shown here there is no change in model constants as there was in the FlexPDE results where C_μ was dependent on Re_τ. All simulations were performed with parameters provided in Table 2 and 18 wave number bins.

4.2.1 Meshing

The numerical mesh setup used to test the SCTM thus far is essentially 1D since boundary lower growth occurs off of the lower wall and the other three walls of the duct are assigned symmetry (no-slip) boundary conditions in NPHASE-CMFD. Figure 16(a) shows the cross-sectional view of a numerical mesh with 48 elements in the direction parallel to the solid wall boundary and Figure 16(b) shows how the stream wise velocity and TKE compare for this 48 element mesh with a higher resolution mesh with 199 elements in the direction parallel to the solid wall boundary. Clearly, the predictions are nearly

identical. All of the following results shown here were simulated on the lower resolution mesh with 48 elements in the direction normal to the solid wall boundary.

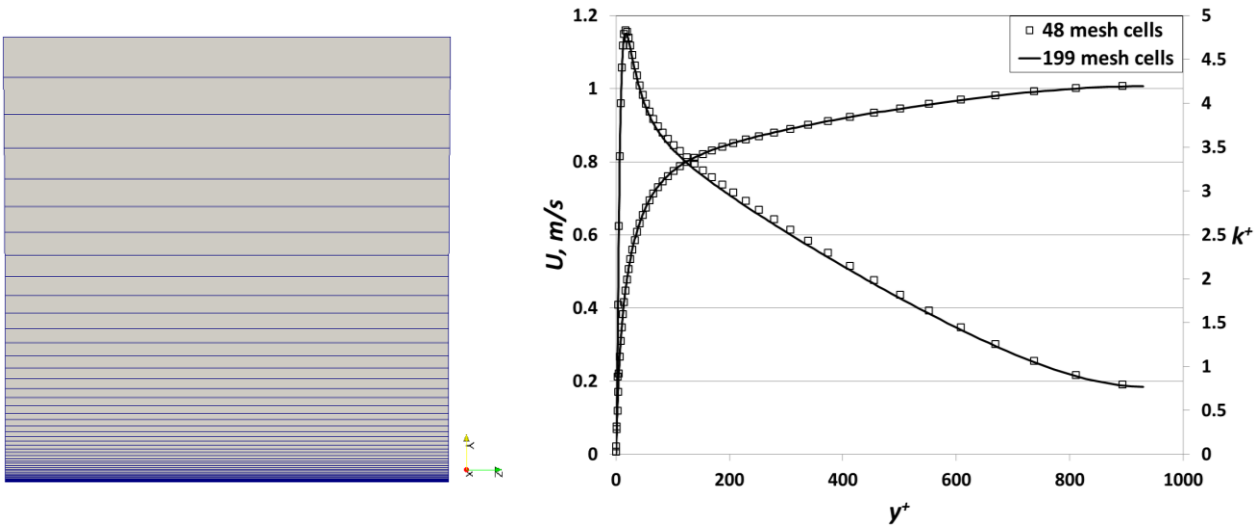

(a) (b)

Figure 16. (a) Cross-sectional view of a numerical mesh with 48 cells in the direction parallel to the wall boundary. (b) Stream wise velocity (left vertical axis) and non-dimensional TKE (right vertical axis) predicted by SCTM in NPHASE-CMFD using two different mesh resolutions (N = 5, Re_τ= 950).

4.2.2 Re_τ = 2000

SCTM predictions using NPHASE-CMFD for the highest considered Reynolds number case are shown in Figure 17 – Figure 19 in comparison to previously shown SCTM predictions using FlexPDE and the DNS data. Most notably, the SCTM with improved inhomogeneous dissipation term implemented into NPHASE-CMFD provides exceedingly better results for the TKE (Figure 17(b)). Results for stream wise velocity (Figure 17(a)) and turbulent viscosity (Figure 18(a)) are on par with estimates from FlexPDE although the location of the turbulent viscosity peak is not predicted as well while the peak magnitude is better captured. The total turbulent dissipation shape (Figure 18(b)) is captured better as well and much improved from the previous result with FlexPDE (Figure 7(d)). The SCTM is somewhat able to capture the inflection point in the turbulent dissipation shape around y^+= 10. The total spectral transfer term sums to zero as expected and does not contribute to the overall TKE budget. Note that the viscous/turbulent diffusion terms are not included in the total source terms plot (Figure 18(b)) since only the turbulence production, homogeneous dissipation, inhomogeneous dissipation, and spectral transfer terms are the user-defined functions supplied to NPHASE-CMFD (see Eq. (20)).

Spectral energy results are shown at two y^+ locations in Figure 19 and the SCTM predictions using NPHASE-CMFD are very similar to those from FlexPDE. There is still some discrepancy closer to the wall (Figure 19(a)) where there is a build-up of energy in the high wave number range. Although the dissipation shape is much better represented with the new formulation for inhomogeneous dissipation the

SCTM still fails to capture the change in energy spectrum slope in the transition from the inertial subrange to the dissipation range for the Re_τ= 2000 case.

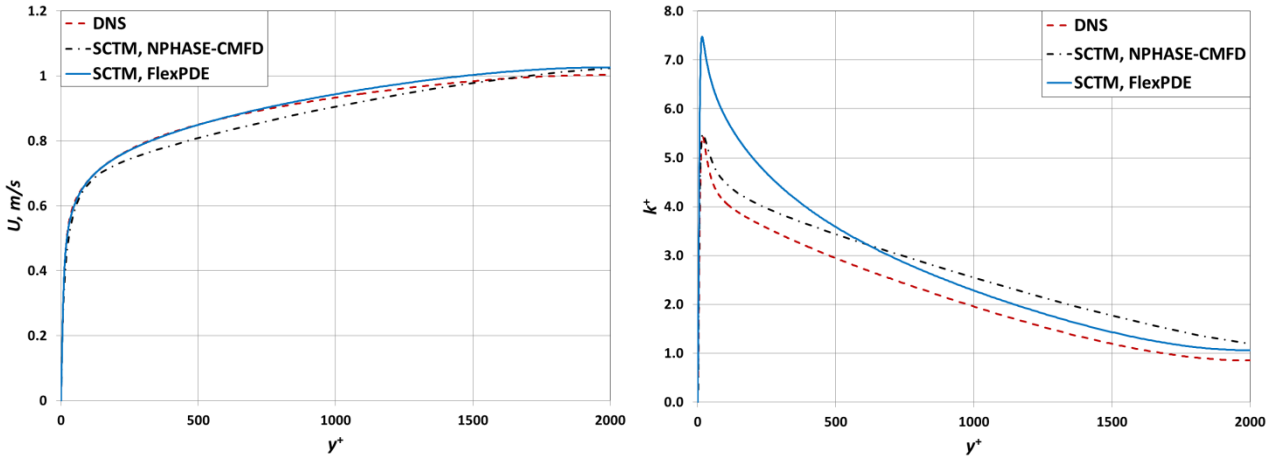

(a) (b)

Figure 17. SCTM predictions (N = 18, Re_τ= 2000) of stream wise velocity (a) and TKE (b) using NPHASE-CMFD (black dashed dot line) in comparison to SCTM prediction using FlexPDE (solid blue line) and DNS data (red dashed line) of Hoyas and Jiminez (2006).

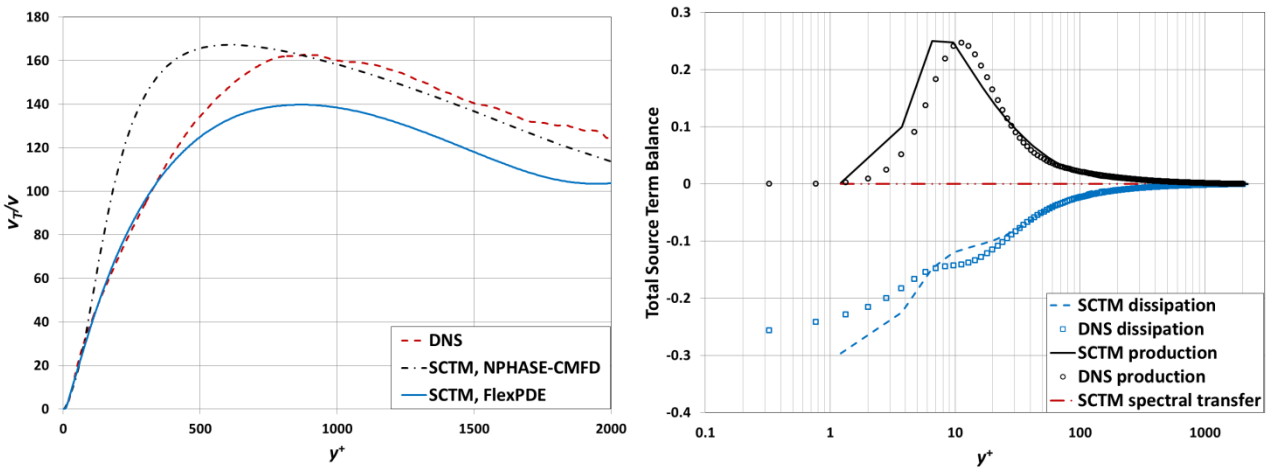

(a) (b)

Figure 18. (a): SCTM prediction (N = 18, Re_τ= 2000) of turbulent viscosity in comparison to SCTM prediction using FlexPDE (solid blue line) and DNS data (red dashed line) of Hoyas and Jiminez (2006). (b): Total source term balance of SCTM using NPHASE-CMFD in comparison to DNS data of Hoyas and Jiminez (2006).

4.2.3 Re_τ = 950

SCTM predictions using NPHASE-CMFD are similar to those from FlexPDE for Re_τ= 950 for the stream wise velocity (Figure 20(a)) while the TKE is better predicted (Figure 20(b)). Although the turbulent viscosity magnitude prediction is further from the DNS data using NPHASE-CMFD (Figure 21(a)) the shape of the DNS curve is better modeled using NPHASE-CMFD. The total source term

balance shows (Figure 21(b)) that the production peak is slightly closer to the wall than the DNS data. However, as with the higher Reynolds number case discussed previously, the new formulation for inhomogeneous dissipation provides a vastly improved prediction of the overall shape of the turbulence dissipation curve from DNS and again is able to capture the deflection point in the curve around y^+= 10. The overall spectral transfer term sums to zero as expected and does not contribute to the TKE budget.

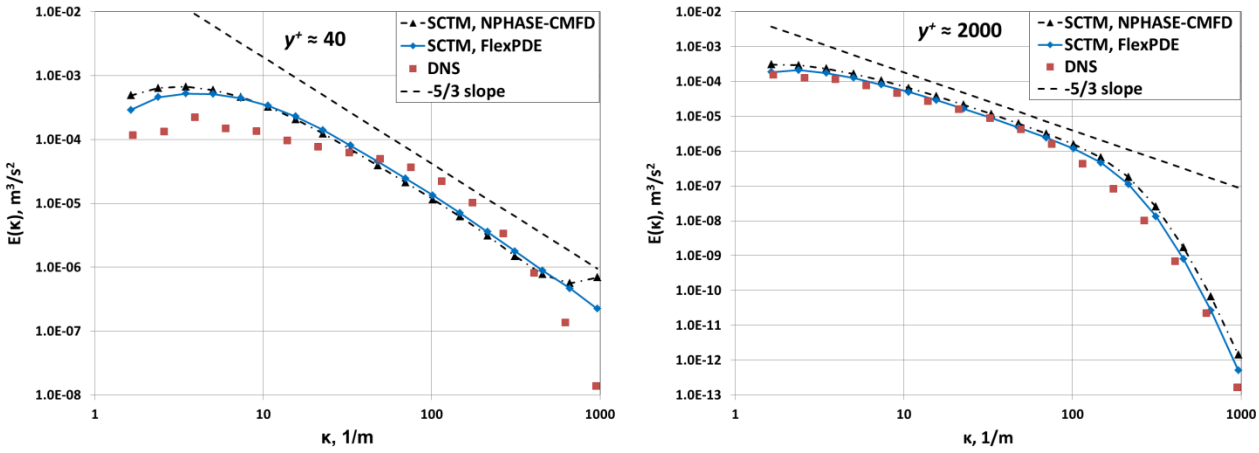

(a) (b)

Figure 19. SCTM (N = 18, Re_τ= 2000) prediction of the TKE spectrum using NPHASE-CMFD (black triangles) and FlexPDE (blue diamonds) in comparison to the DNS data (red squares) and -5/3 slope (dashed line) at y^+= 40 (a) and y^+= 2000 (b).

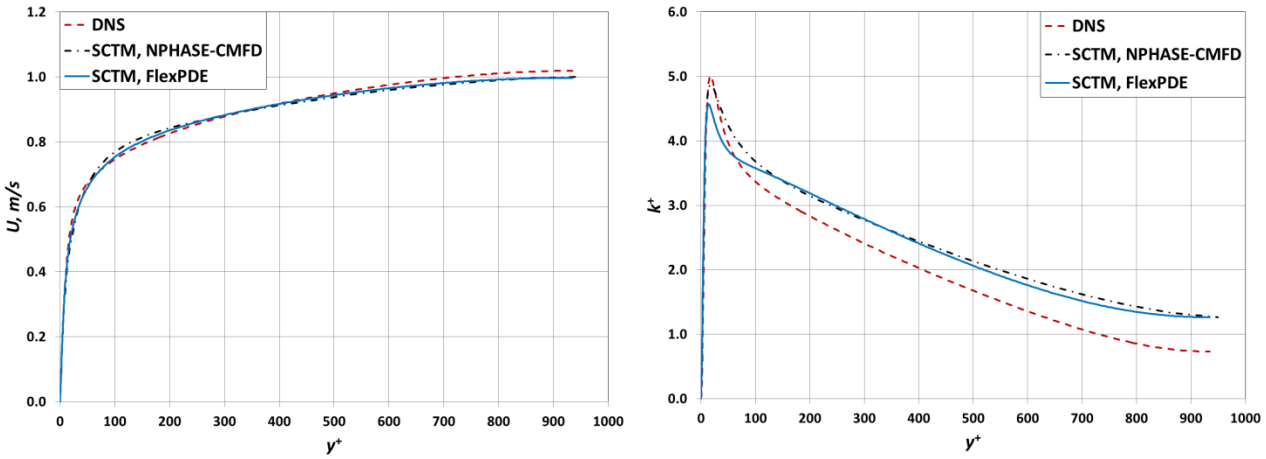

(a) (b)

Figure 20. SCTM prediction (N = 18, Re_τ= 950) of stream wise velocity (a) and TKE (b) using NPHASE-CMFD (black dashed dot line) in comparison to SCTM prediction using FlexPDE (solid blue line) and DNS data (red dashed line) of del Alamo et al. (2004).

Spectral energy results at Re_τ= 950 are shown in Figure 22 for two different distances from the solid wall boundary. The SCTM results from NPHASE-CMFD are very close to those from FlexPDE. Although the model formulation has been slightly altered between predictions from the two numerical

tools the similar behavior is encouraging numerical verification that the SCTM performance in the 3D M-CFD code is as expected.

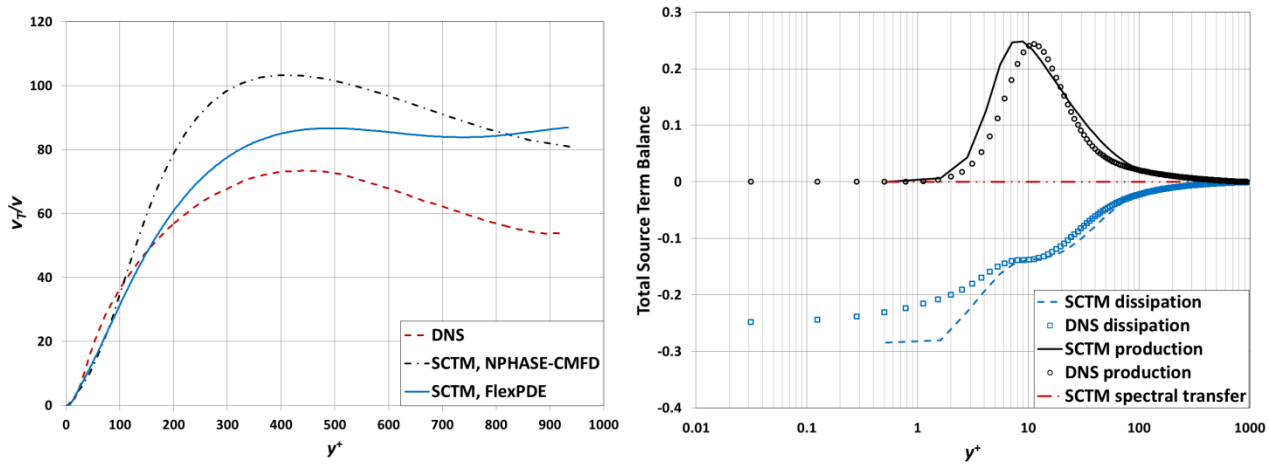

(c) (d)

Figure 21. (a): SCTM prediction (N = 18, Re_τ= 950) of turbulent viscosity in comparison to SCTM prediction using FlexPDE (solid blue line) and DNS data (red dashed line) of del Alamo et al. (2004). (b): Total source term balance of SCTM using NPHASE-CMFD in comparison to DNS data of del Alamo et al. (2004).

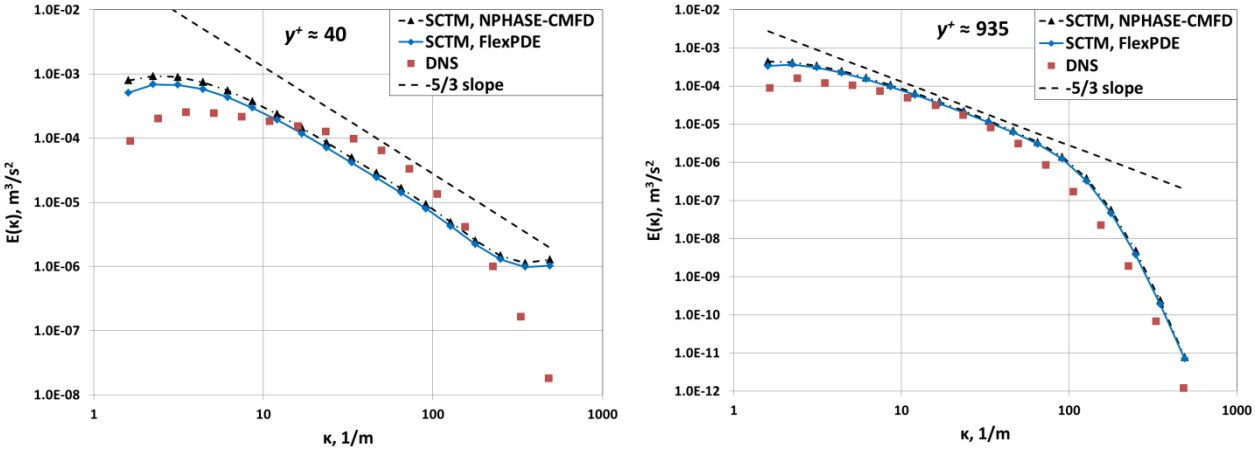

(a) (b)

Figure 22. SCTM (N = 18, Re_τ= 950) prediction of the TKE spectrum using NPHASE-CMFD (black triangles) and FlexPDE (blue diamonds) in comparison to the DNS data (red squares) and -5/3 slope (dashed line) at y^+= 40 (a) and y^+= 935 (b).

4.2.4 Re_τ = 550

The general trends for the higher Reynolds number cases discussed previously are seen for the SCTM predictions using NPHASE-CMFD at Re_τ= 550 (Figure 23 – Figure 25). Note that at this Reynolds number the TKE peak is well-predicted (Figure 23(b)) and turbulence dissipation shape is very well modeled by the SCTM (Figure 24(b)). Spectral energy results at two different y^+ locations show

very similar results for NPHASE-CMFD and FlexPDE. However, at this Reynolds number the energy build-up in the high wave number range for the location close to the wall is slightly less for the NPHASE-CMFD results than for the FlexPDE results. It is possible that significantly increasing the number of spectral bins could mitigate this build-up of energy in the dissipation range although the spectral resolution for each of these cases is less than the maximum suggested value of 2.

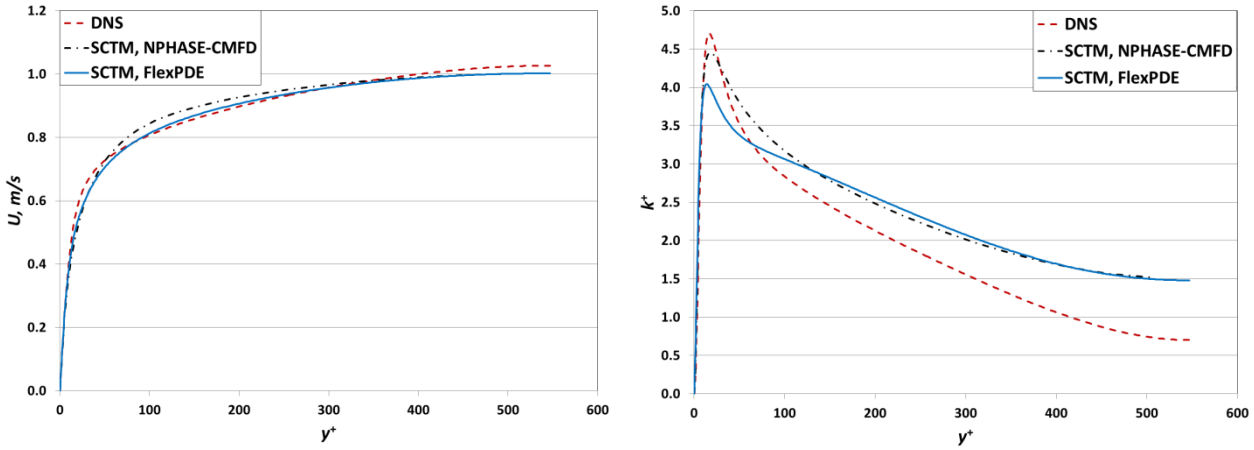

(a) (b)

Figure 23. SCTM predictions (N = 18, Re_τ= 550) of stream wise velocity (a) and TKE (b) using NPHASE-CMFD (black dashed dot line) in comparison to SCTM prediction using FlexPDE (solid blue line) and DNS data (red dashed line) of del Alamo and Jiminez (2003).

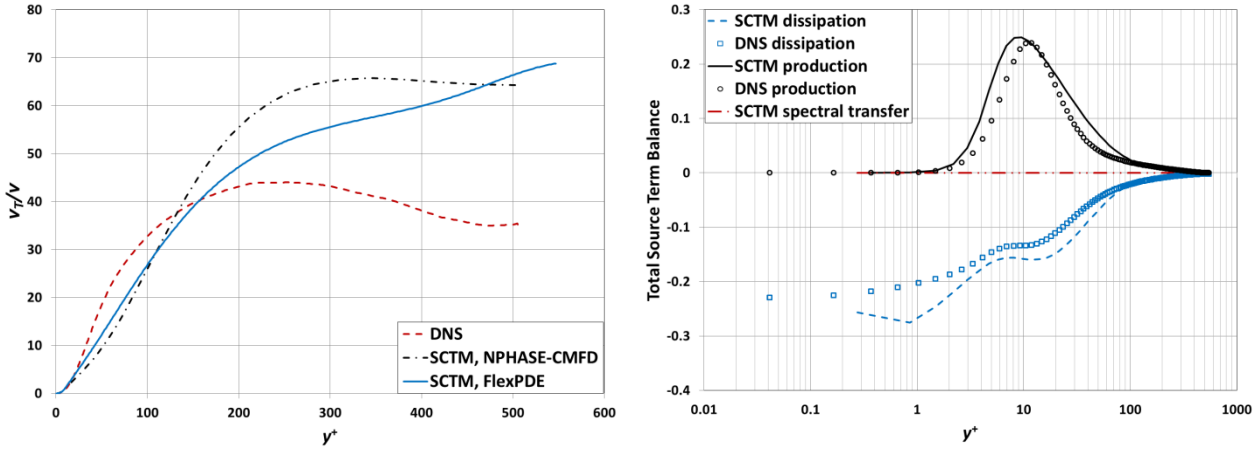

(a) (b)

Figure 24. (a): SCTM prediction (N = 18, Re_τ= 550) of turbulent viscosity in comparison to SCTM prediction using FlexPDE (solid blue line) and DNS data (red dashed line) of del Alamo and Jiminez (2003). (b): Total source term balance of SCTM using NPHASE-CMFD in comparison to DNS data of del Alamo and Jiminez (2003).

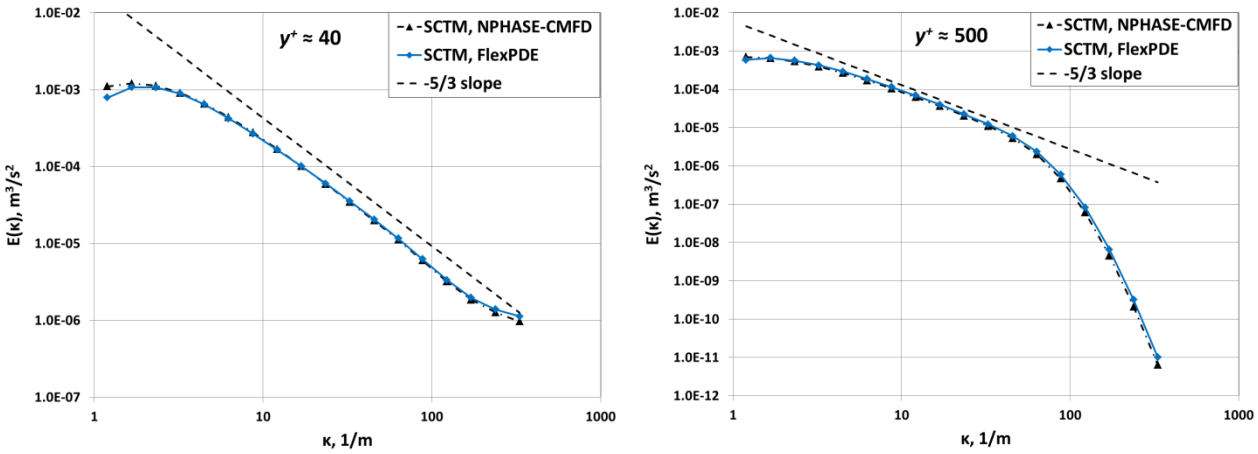

(a) (b)

Figure 25. SCTM (N = 18, Re_τ= 550) prediction of the TKE spectrum using NPHASE-CMFD (black triangles) and FlexPDE (blue diamonds).

5 CONCLUSIONS

The spectral cascade-transport turbulence model presented herein satisfactorily predicts the mean velocity, TKE profiles, and the TKE spectrum for single-phase turbulent channel flows with Reynolds numbers up to 2000 based on friction velocity (Re_τ= 2000, Re_δ= 31000). The model is robust, with good predictions of mean flow quantities and the energy spectrum even for a low number of spectral bins. The current work extends SCTM capabilities; resolving the turbulence all the way to the wall as well as recovering the -5/3 slope in the inertial subrange of the energy spectrum for higher Reynolds number flows. The current work also conducts a first test in implementing the SCTM to be a turbulence closure option in the 3D M-CFD code NPHASE-CMFD through a repurposing of existing code structure. Based on the promising results in the current work an array of test cases pertinent to the expected multiphase flow scenarios in nuclear reactor subchannels need to be designed and performed to fine tune and finalize model constants.

As in previous studies (Bolotnov et al., 2008a,Bolotnov et al., 2008b) this turbulence model for wall bounded flows has the potential to also predict two-phase turbulence for bubbly flows (Bolotnov et al., 2009) with better physical representations of bubble/turbulence interactions in different scales than existing non-spectral models. Extending the wall-resolved SCTM to multiphase flows will not require multiphase law of the wall type boundary conditions as the previous work (Bolotnov et al., 2009) would, eliminating a major source of modeling uncertainty. Capabilities of the SCTM to provide good mean flow predictions even for bin resolutions higher than the suggested $\xi = 2$ results in more flow statistics (e.g. the energy spectrum) for minimal increases in computational cost.

6 ACKNOWLEDGEMENT

The authors would like to acknowledge the support from Consortium for Advanced Simulation of Light Water Reactors (http://www.casl.gov), an Energy Innovation Hub (http://www.energy.gov/hubs) for Modeling and Simulation of Nuclear Reactors under U.S. Department of Energy [grant number DE-AC05-00OR22725].

7 REFERENCES

Bohr, T., Jensen, M.H., Paladin, G., Vulpine, A., 1998. A Dynamical Systems Approach to Turbulence. Cambridge University Press.

Bolotnov, I.A., Lahey, R.T.,Jr., Drew, D.A., Jansen, K.E., 2008a. Turbulent cascade modeling of single and bubbly two-phase turbulent flows. Int. J. Multiphase Flow 34, 1142-1151.

Bolotnov, I.A., Lahey, R.T.,Jr., Drew, D.A., Jansen, K.E., Oberai, A.A., 2008b. A spectral turbulent cascade model for single- and two-phase uniform shear flows. Journal of Turbulence 9, 1-18.

Bolotnov, I.A., Lahey, R.T., Drew, D.A., Jansen, K.E., Oberai, A.A., 2009. Spectral cascade modeling of turbulent flow in a channel. Japanese Journal of Multiphase Flow 23, 190-204.

Bolotnov, I.A., Lahey, R.T., Jr., Drew, D.A., Jansen, K.E., Oberai, A.A., 2010. Spectral analysis of turbulence based on the DNS of a channel flow. Comput. Fluids 39, 640-655.

Bradbury, L.J.S., Durst, F., LAUNDER, B., Schmidt, F.W., 1980. Multiple-time-scale concepts in turbulent shear flows, in Anonymous Turbulent Shear Flows. Springer-Verlag, New York, pp. 36-49.

Brown, C.S., Bolotnov, I.A., 2016. Spectral analysis of single- and two-phase bubbly DNS in different geometries. Nuclear Science and Engineering 184, 363-376.

Cadiou, A., Hanjalic, K., Stawiarski, K., 2004. A two-scale second-moment turbulence closure based on weighted spectrum integration. Theor. Comput. Fluid Dyn. 18, 1-26.

CHIEN, K., 1982. Predictions of Channel and Boundary-Layer Flows with a Low-Reynolds-Number Turbulence Model. AIAA J. 20, 33-38.

Del Alamo, J.C., Jimenez, J., Zandonade, P., Moser, R.D., 2004. Scaling of the energy spectra of turbulent channels. J. Fluid Mech. 500, 135-144.

del Alamo, J., Jimenez, J., 2003. Spectra of the very large anisotropic scales in turbulent channels. Phys. Fluids 15, L41-L44.

Desnyanski, V.N., Novikov, E.A., 1974. Simulation of cascade process in turbulent flows. Journal of Applied Mathematics and Mechanics 38, 216.

Fang, J., Rasquin, M., Bolotnov, I.A., 2016. Interface tracking simulations of bubbly flows in PWR relevant geometries. Nuclear Engineering and Design .

GLEDZER, E., 1973. System of Hydrodynamic Type Allowing 2 Quadratic Integrals of Motion. Dokl. Akad. Nauk SSSR 209, 1046-1048.

Hinze, J.O., 1975. Turbulence. McGraw-Hill, New York.

Hoyas, S., Jimenez, J., 2006. Scaling of the velocity fluctuations in turbulent channels up to Re-tau=2003. Phys. Fluids 18, 011702.

Interphase Dynamics, L., 2002. NPHASE-CMFD User Manual.

JONES, W., LAUNDER, B., 1972. Prediction of Laminarization with a 2-Equation Model of Turbulence. Int. J. Heat Mass Transfer 15, 301-&.

KIM, S., 1990. Near-Wall Turbulence Model and its Application to Fully-Developed Turbulent Channel and Pipe Flows. Numer Heat Tranf. B-Fundam. 17, 101-122.

KIM, S., CHEN, C., 1989. A Multiple-Time-Scale Turbulence Model Based on Variable Partitioning of the Turbulent Kinetic-Energy Spectrum. Numer Heat Tranf. B-Fundam. 16, 193-211.

LAHEY, R., DEBERTODANO, M., JONES, O., 1993. Phase Distribution in Complex-Geometry Conduits. Nucl. Eng. Des. 141, 177-201.

LEWALLE, J., TAVLARIDES, L., 1994. A Cascade-Transport Model for Turbulent Sheer Flows. Phys. Fluids 6, 3109-3115.

OHKITANI, K., YAMADA, M., 1989. Temporal Intermittency in the Energy Cascade Process and Local Lyapunov Analysis in Fully-Developed Model Turbulence. Prog. Theor. Phys. 81, 329-341.

PDE Solutions Inc, FlexPDE. Finite element analysis software package.

Pope, S.B., 2000. Turbulent Flows. Cambridge University Press, Cambridge ;New York.

SCHIESTEL, R., 1987. Multiple-Time-Scale Modeling of Turbulent Flows in One Point Closures. Phys. Fluids 30, 722-731.

Trofimova, A.V., Tejada-Martinez, A.E., Jansen, K.E., Lahey, R.T., Jr., 2009. Direct numerical simulation of turbulent channel flows using a stabilized finite element method. Comput. Fluids 38, 924-938.

WILCOX, D., 2002. Turbulence Modeling for CFD. DCW Industries, La Canada, CA.